GLASS-LIKE, LOW-ENERGY EXCITATIONS IN NEUTRON-IRRADIATED QUARTZ

BY

JOHN WILLIAM GARDNER

A.B., Princeton University, 1976
M.S., University of Illinois, 1978

THESIS

Submitted in partial fulfillment of the requirements
for the degree of Doctor of Philosophy in Physics
in the Graduate College of the
University of Illinois at Urbana-Champaign, 1980

Urbana, Illinois

DISCLAIMER

GLASS-LIKE, LOW-ENERGY EXCITATIONS IN NEUTRON-IRRADIATED QUARTZ

BY

JOHN WILLIAM GARDNER

A.B., Princeton University, 1976
M.S., University of Illinois, 1978

THESIS

Submitted in partial fulfillment of the requirements
for the degree of Doctor of Philosophy in Physics
in the Graduate College of the
University of Illinois at Urbana-Champaign, 1980

Urbana, Illinois

GLASS-LIKE, LOW-ENERGY EXCITATIONS IN NEUTRON-IRRADIATED QUARTZ

John William Gardner, Ph.D.
Department of Physics
University of Illinois at Urbana-Champaign, 1980

The specific heat and thermal conductivity of neutron-irradiated crystalline quartz have been measured for temperatures $\tilde{}$ 0.1-5 K. Four types of low-energy excitations are observed in the irradiated samples, two of which can be removed selectively by heat treatment. One set of remaining excitations gives rise to low-temperature thermal behavior characteristic of glassy (amorphous) solids. The density of these glass-like excitations can be 50% the density observed in vitreous silica, yet the sample still retain long-range atomic order. In a less-irradiated sample, glass-like excitations may be present with a density only $\tilde{}$ 2.5% that observed in vitreous silica and possess a similar broad energy spectrum over 0.1-1 K.

ACKNOWLEDGMENTS

Dr. Terry Smith kindly assisted with the sample irradiations and J. McMillan performed the x-ray analysis.

The author thanks Dr. A. C. Anderson for suggesting the present research and particularly thanks him for his absolutely unfailing interest and helpfulness.

This work was supported in part by the U.S. Department of Energy under Contract DE-AC02-76ER01198.

TABLE OF CONTENTS

I. INTRODUCTION

A. Glasses at Low Temperatures

Since the advent of low temperature capability in the 1960's, it has been observed that amorphous solids (synonymously, glasses) exhibit, at temperatures $\lesssim 1$ K, characteristic thermal and ultrasonic properties quite different from those of crystalline solids.[1,2] In particular, there is a large specific heat above the phonon contribution observed in crystals, and this excess specific heat varies approximately as the temperature, T. It is also found that the magnitude of the excess specific heat is remarkably similar among glasses (this includes[1,3,4] inorganics, polymers, semiconductors, and metals). The thermal conductivity is likewise similar among glasses, is much less than that of a similarly sized crystal, and varies approximately as T^2 (for $T \lesssim 1$ K), see Fig. 1. Glasses exhibit strong ultrasonic attenuation at low ultrasonic input powers and saturation effects at higher powers.

In 1972 a model[5,6] was put forth which accounted for all of the low-temperature properties of glasses in a simple though phenomenological way: there exist throughout the glass, it is presumed, localized, two-level excitations which have coupling to the lattice. Ultrasonic attenuation comes about through resonant absorption by these excitations, and a saturation in attenuation follows naturally at higher powers. For the thermal properties, some density of states, n(E) (where E is the energy difference of the two

Figure 1. (a) Specific heat C (divided by T^3 to emphasize the departure from the phonon contribution) and (b) thermal conductivity κ versus temperature T of vitreous silica (glassy SiO_2) and quartz (crystalline SiO_2). Below 1 K, perfect crystals exhibit a $C \propto T^3$ and $\kappa \propto T^3$; glasses, $C \propto T$ and $\kappa \propto T^2$.

Z: Zeller and Pohl (Ref. 7)
S: Stephens (Refs. 1,8)
F: Flubacher, et al. (Ref. 9)
B: Bilir and Phillips (Ref. 10)
κ data from Ref. 11.

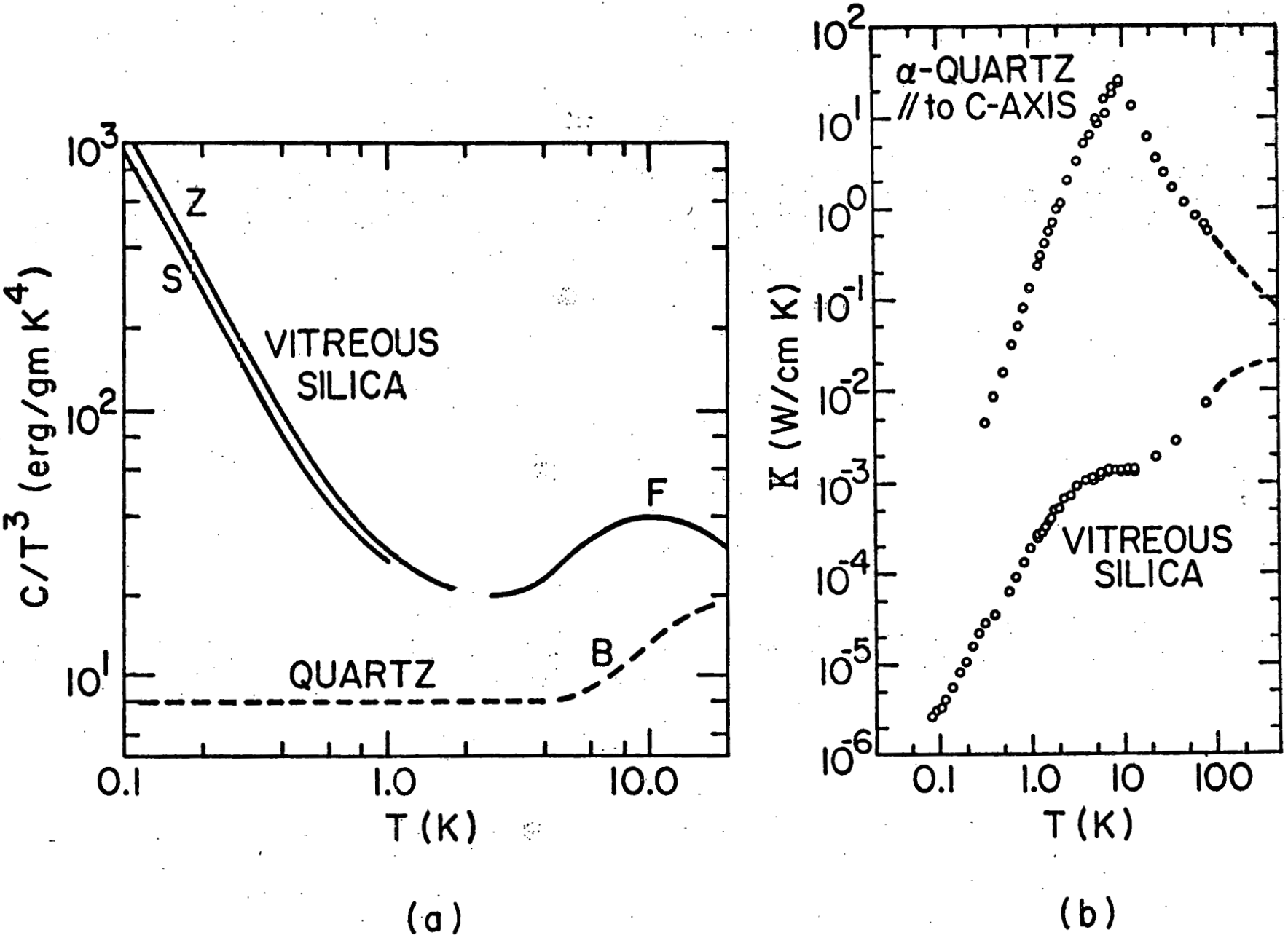
10^3
10^2
10^1
C/T^3 (erg/gm K^4)
Z
S
VITREOUS
SILICA
F
B
QUARTZ
0.1
1.0
10.0
T (K)
(a)
10^2
10^1
10^0
10^{-1}
10^{-2}
10^{-3}
10^{-4}
10^{-5}
10^{-6}
K (W/cm K)
α-QUARTZ
// to C-AXIS
VITREOUS
SILICA
0.1
1.0
10
100
T (K)
(b)

levels), must be chosen for these excitations, and if an energy-independent density is assumed, $n(E) = n_o$, the specific heat will be linear in temperature and the thermal conductivity quadratic in temperature. The theory is named the tunneling-states model since it proposes that the excitation is the split ground state of a mass (e.g., an atom or group of atoms) which can tunnel between two potential wells. Presumably in the amorphous structure such double well configurations could occur; for example, as a "bend left" or "bend right" position of an atom with two connecting bonds. Symmetry would rule out this degeneracy in a perfect crystal. However, identification of a tunneling entity has not been made for any glass. This is not to say tunneling states in solids with energy splittings in the range of interest ($E \lesssim 1$ K: energy in Kelvin units) have not been observed. Substitutional impurities in alkali halides have been shown to tunnel in some instances,[12] and also to interact strongly with the lattice, thus lowering the thermal conductivity.

Another feature of glasses which has not been understood is why the density of states n(E) should be nearly constant over a large range of energies, from at least 0.01-1 K. The tunneling-states model makes no explanation of this, but assumes rather the distribution ad hoc to produce the observed results. In 1978 Klein, et al.,[13] calculated the effect of strain interactions among tunneling systems in a glass and found that the inclusion of strain interactions would serve to broaden an n(E) which, in the absence of strains, could be as sharp as δ-functions. Furthermore, if the tunneling systems are of sufficient concentration,

the density of states will become, at low energies, independent of the tunneling-system concentration. Thus the strain broadening model provides a possible explanation for the universal magnitude of thermal properties observed in glasses. In vitreous silica, the concentration of tunneling systems above which n(E) should be concentration-independent is calculated to be $\approx 10^{20}$ cm^{-3}, and, if the tunneling-states model is assumed, there is evidence[14] that there are as many as 2×10^{20} cm^{-3} tunneling systems present. This corresponds to about 0.1% of the oxygen atoms. Thus the theory may account for the density of states observed in vitreous silica. However, there has been no independent confirmation that this mechanism actually is responsible for the broad, universal n(E) observed in glasses.

B. Motivation for the Present Work

Early in the 1950's Berman[15] measured the thermal conductivity of neutron-irradiated quartz for temperatures down to 5 K. With increasing neutron dose, the thermal conductivity was shown to drop from the high peak at 5-10 K characteristic of crystals (see Fig. 1; the Berman data are shown in Fig. 6) to a much reduced, nearly temperature-independent region in the same temperature range. Such "plateaus" in the thermal conductivity near 10 K are characteristic of glasses, although the cause of the plateau is not understood. In particular, it is not known whether the plateau is caused by the presumed tunneling excitations which dominate the thermal properties below 1 K. However, the apparent transformation of crystalline quartz to a glass-like material raises interesting questions:

(1) It is known[16] that for a fast-neutron ($E_{neutron} \gtrsim 0.1$ MeV) dose $\lesssim 3 \times 10^{19}$ cm^{-2}, quartz remains crystalline, i.e., no significant change in the sharpness of x-ray reflections is observed. At exposures $\gtrsim 2 \times 10^{20}$ cm^{-2} the material is completely vitrified.[17] Can the glass-like excitations exist in the neutron-damaged crystalline material (i.e., exposure $\lesssim 3 \times 10^{19}$)? If so, with a better understanding of the damage created by a fast neutron and of the crystalline environment, the excitation might be identified.

(2) Indeed, how might n(E) form at intermediate neutron exposures? According to the strain broadening model, a concentration of tunneling systems a factor ~ 10 less than that presumably present in vitreous silica need not possess a broad n(E). If n(E) were a sharp function of energy, a test of the tunneling model for the excitations and identification of the tunneling entity could possibly be made by an isotope effect, as was done[12] for substitutional impurities in alkali halides. Also, if n(E) were sharp for some neutron dose and if strain interaction broadening is a dominate process, a spreading of n(E) might be observed at higher dosage.

The present experiments were begun to probe n(E) of neutron-irradiated quartz for several values of neutron dose by measurements of specific heat and thermal conductivity at temperatures down to ≈ 0.1 K. Since then, additional information has become available.

Laermans[18] measured the ultrasonic attenuation in quartz exposed to $\approx 6 \times 10^{18}$ cm^{-2} fast neutrons and observed saturation as in a glass. The coupling constant[14,19] of the attenuating excitations to the lattice was also measured[20] and found to be approximately that measured in vitreous silica. X-ray analysis confirmed the material was still crystalline. Additionally,[21] the thermal conductivity of the sample was measured down to 1.4 K and seemed to approach a T^2 dependence. The present experiments will confirm that glass-like excitations are present in neutron-damaged crystalline quartz, and may be produced with a density as much as a factor of 40 smaller than the density in vitreous silica. The spectrum, n(E), of the excitations is broad even at this low concentration; therefore it is possible that the broad, universal n(E) in glasses is not explained by the strain interactions model.

A further comment should be made. A major point of ignorance in this course of investigation, at least at the present time, is the precise nature of neutron-induced damage in crystals. For instance, it is not known with certainty even how large a region is damaged when a fast neutron ($\sim$1 MeV) collides with a nucleus in the solid, although it is believed[22,23] that a "damage cluster" of perhaps 10^4 atoms is formed. Also, there obviously is no guarantee that, even if glass-like excitations are produced, other excitations might not also be produced which completely dominate the low-temperature properties. In fact, this problem was encountered to varying degree in the present work, but fortunately, recent other work has aided in the classification if not explanation of the

near menagerie created by reactor neutron irradiation. Here we also will discuss each "extraneous" effect or excitation in turn in order to pinpoint the evidence for glass-like excitations and to provide a guide for future research. A more definitive understanding of the microscopic nature of the glass-like excitations is hoped for when neutron damage is better characterized.

II. SAMPLE CHARACTERIZATION AND EXPERIMENTAL PROCEDURE

A. Irradiations

Five samples measuring 1 cm x 0.4 cm x 5 cm (a:b:c) were cut from adjacent positions of a single crystal[24] of electronic-grade cultured α-quartz. Emission spectroscopy showed the samples contain ≈4 ppm (wt.) Al, ≈20 ppm (wt.) Ca, < 5 ppm (wt.) Fe and Mn, < 20 ppm (wt.) Ni and Co, and < 1 ppm (wt.) Cu. The Al and Ca values are accurate to a factor of 3, and the upper values are limits on the spectroscopy sensitivity. One sample was reserved and four were irradiated in the CP-5 reactor[25] at Argonne National Laboratory for 3 h, 27 h, 270 h, and 2100 h, respectively. The samples will henceforth be designated 0 h (unirradiated), 3 h, 27 h, 270 h, and 2100 h. For the irradiation the samples were wrapped in aluminum foil and placed in perforated aluminum cans; hence the samples were in direct thermal contact with the cooling water of the reactor. Table 1 shows the neutron dose each sample received in different neutron energy ranges. As the mean free path of a neutron in SiO_2 is ≈10 cm, the samples were irradiated uniformly. The γ exposure was $\sim 10^6$ R/h (average energy ~1 MeV); the β exposure is not known. Following irradiation, the samples were etched in hydrofluoric acid to remove surface contamination.

Before irradiation, the samples (upon wetting the optically rough surface) were colorless and transparent to the eye. After irradiation the 2100 h sample was uniformly bluish, the 270 h

TABLE 1. Radiation dose, mass density, and appearance of samples after exposure to neutron radiation and after heat treatment at 370°C and 840°C.

Sample:	0 h	3 h	27 h	270 h	2100 h
dose (cm^{-2}) 0-0.5 eV	-	5.8×10^{17}	5.3×10^{18}	4.7×10^{19}	4.1×10^{20}
dose (cm^{-2}) 0.5 eV - 0.1 MeV	-	2.2×10^{17}	2.0×10^{18}	1.9×10^{19}	1.5×10^{20}
dose (cm^{-2}) 0.1 MeV-∞	-	2.9×10^{17}	2.7×10^{18}	2.6×10^{19}	2.1×10^{20}
density (g/cm^3)	2.651	2.648	2.640	2.517	2.256
coloration	clear	central smoky	central tan	light tan	blue
after 370°C anneal:					
coloration	-	central light gray	-	dark tan	green
after 840°C anneal:					
coloration	central blue in reflection	central blue in reflection	central blue in reflection	clear	-
density (g/cm^3)	2.651	2.650	2.650	2.520	-

was uniformly light tan, the 27 h was dark tan in a central trapezoidal region (see inset Fig. 4 in Chap. III) and light tan outside this region, and the 3 h sample was smoke-colored (gray-black) in an identical central region and clear outside. The color pattern of the 27 h and 3 h samples was not caused by inhomogeneous exposure in the reactor.[26] Also, the impurity content in the central region did not differ significantly from that in the outer region. The visual appearances are summarized in Table 1, along with mass densities measured to an accuracy of 0.1%.

B. Heat Treatments

Experiments were also performed on the samples after heat treatment at 370°C and again at 840°C in an argon atmosphere. For the 370°C anneal, the sample was brought to temperature in 15 min, held at 370°C for 2 h, then cooled to room temperature in ≈20 min. For the 840°C anneal the sample was brought to temperature in ≈1 h, then allowed to cool, reaching 500°C in 20 min and ≈200°C in 1.5 h. Color and density changes of the heat-treated samples are listed in Table 1.

C. Thermal Conductivity

Thermal conductivities were measured with the heat flux directed parallel to the crystalline c-axis. See Fig. 2. The temperature gradient created by the heater was measured with precalibrated germanium thermometers to eliminate uncertainty in temperatures from radioactive self-heating effects. The thermal conductivity, κ, is given by

Figure 2. Thermal conductivity configuration.[27]

(a) The 0.16 cm thick copper plate G is bolted to the refrigerator at point R and provides thermal grounding for the sample S through copper arm G'. Thermal contact between S and G' is made through the coil-foil joint J. Two precalibrated germanium thermometers, T_1 and T_2, are bolted to strain hardened (stretched) #22 copper wires M_1 and M_2, which are epoxied to the sample with Scotchcast 8 epoxy resin. One end of the sample is attached to 0.01 cm thick copper foil F with GE 7031 varnish. The heater, H, consists of a 120 ohm strain gage varnished onto F. Electrical leads (not shown) from T_1, T_2, and H to plate G are made from superconducting niobium wire which has a much higher thermal resistance than sample S and joint J.

(b) Side view detail of the joint J. Coil-foil C is soldered to the copper arm G' and folded tightly over the sample S. Thermal contact is facilitated by grease on the sample end and by tying the coil-foil tightly to the sample with string W. P and B are toothpick and Micarta pieces, respectively, placed under the string for a tighter joint.

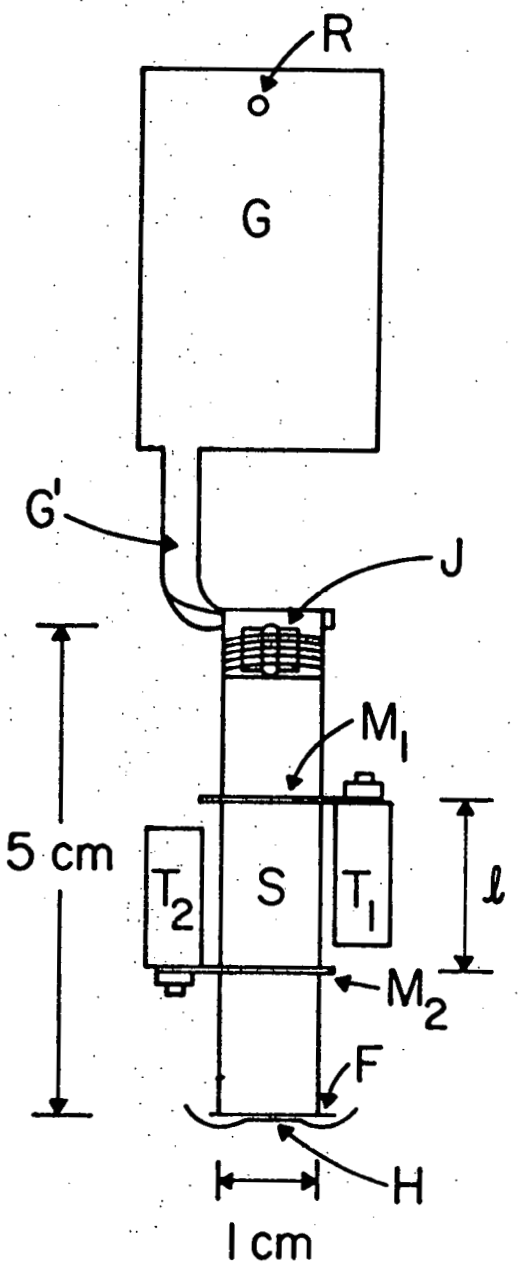

(a)

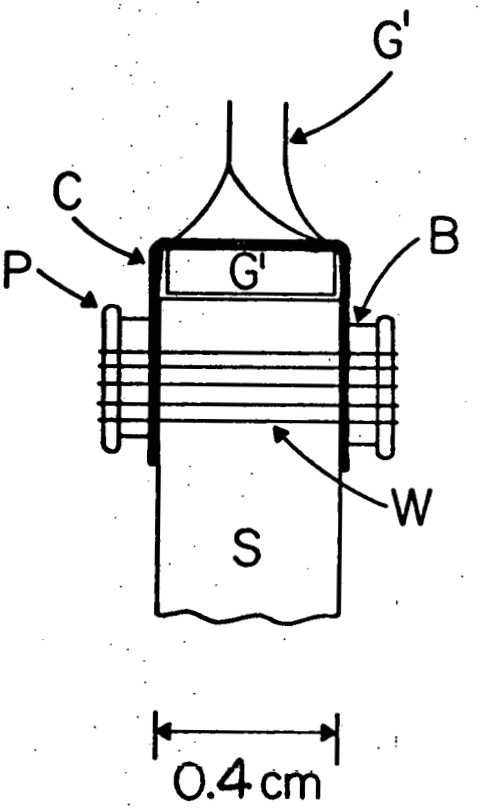

(b)

$$\kappa(\bar{T}) = P\ell A^{-1}(T_{2,on} - T_{2,off})^{-1}, \qquad \bar{T} = (T_1 + T_{2,on})/2,$$

where P is the power supplied to the heater, ℓ is the distance between thermometers, A is the cross-sectional area of the sample, $T_{2,on}$ is the temperature of the thermometer nearer the heater with the power on, $T_{2,off}$ with the power off, and T_1 is the temperature of the other thermometer. For each datum the temperature T_1 is kept constant. $\bar{T}$ gives the average temperature of the sample between the two thermometers. Typically, $(T_{2,on} - T_1)$ was 5-10% of $\bar{T}$.

The uncertainty in the thermal conductivity data arises mainly from uncertainty in ℓ and A, which were determined to 2% and 1%, respectively. The power P was measured to $\approx 0.3\%$. Therefore, the overall uncertainty in κ is ≈ 3-4%. The temperature $\bar{T}$ is much better determined, as temperatures were measured to $\approx 0.2\%$.

D. Specific Heat

Specific heat was measured by two techniques. In one, the sample was isolated from the refrigerator by a weak thermal link and operated as a quasi-adiabatic calorimeter,[28] see Fig. 3(a). A brief current pulse of known duration was supplied to a heater on the sample, and the rise in temperature was monitored by a carbon resistance thermometer. The thermometer is described in Fig. 3(c). The same addenda (viz., thermometer, heater, fishline, and amount of glue) were used for all weak-link experiments. The pulse duration and internal thermal equilibrium time were much less than the external thermal decay time of the sample through the weak link. The specific heat C is given by

$$C(\bar{T}) = Q(V\,\Delta T)^{-1},$$

Figure 3. Specific heat experiments.

(a) Weak-link technique. A 0.20 cm thick copper plate G provides thermal grounding to the refrigerator. The sample S is tightly bound by three loops of 0.033 cm diameter nylon fishing line F to prevent vibrational heating of S and to provide the weak thermal link to the refrigerator. The line is attached to G by greased screws and thermal contact from F to S is ensured by small dots of GE 7031 varnish applied at the points where F comes away from the sample (two points for each loop). Thermometer T is bonded to the sample with varnish. M is a superconducting lead from thermometer T, as described in (c). The heater H consists of a 2.8 cm length of 0.0025 cm diameter platinum/tungsten alloy wire wrapped tightly around the sample and continuously bonded to S with a line of varnish drawn off the tip of a toothpick. Superconducting 0.01 cm diameter niobium leads N were spot-welded to H. The weld joint was also varnished to the sample. The thermal resistances of M and N are much greater than that of F. GE 7031 varnish was the sole bonding agent used on the sample so that the experiment could be disassembled easily with a relatively mild solvent (ethanol) and the same addenda reused. The heater wire, however, was replaced each time (from the same spool).

(b) Diffusivity technique, scale same as in (a). G, S, T, H, N, and M are as described in (a). One end of the sample is epoxied with Scotchcast 8 epoxy resin to a small copper block B. B has a tapped hole extending partially into its interior. A copper screw thermally grounds B to G. This design was chosen so that B and S could be removed from G and soaked in solvent to dissolve the epoxy joint.

(c) Side view close-up of thermometer T. C is a chip of carbon from a Speer 100 ohm resistor with linear dimensions ≈ 0.1 cm. C is epoxied to a 0.0013 cm thick Mylar strip M, ≈ 0.15 cm wide, and some epoxy E is welled up against C to provide a smooth, continuous surface for L. L is a vapor-deposited lead/tin alloy film approximately 3×10^{-5} cm thick. In performing a specific heat experiment, the resistance of T indicates the temperature of the sample.

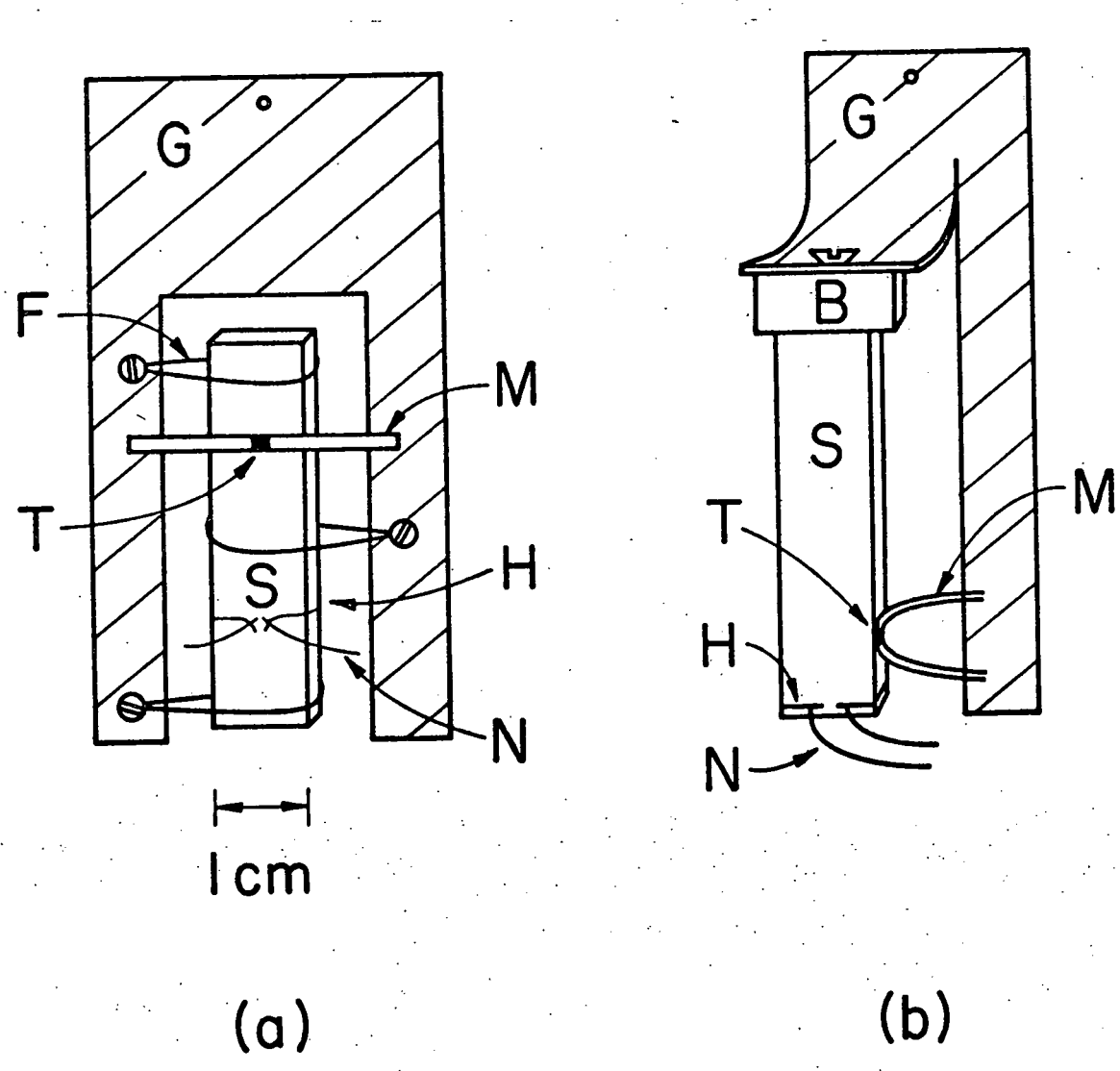
G
F
M
T
S
H
N
1cm
(a)
G
B
S
M
T
H
N
(b)
M
C
E
L
(c)

where Q is the energy dissipated in the heater, V is the volume of the sample, and ΔT is the monitored temperature rise immediately following the current pulse. The average temperature $\bar{T}$ is half the temperature rise ΔT added to the equilibrium temperature with the heater off. ΔT was typically 10% of $\bar{T}$. Determination of ΔT was improved by repeating the experiment several times in sequence and signal averaging.

Uncertainty in the weak-link data arises predominantly from an uncertainty in ΔT, estimated to be 5%. The error introduced into $\bar{T}$ is negligible; therefore the specific heat by the weak-link method is uncertain by $\approx 5\%$.[29]

In the weak-link configuration, sample 270 h could be measured only down to a temperature ≈ 0.4 K and 2100 h only to ≈ 0.7 K due to spontaneous heating of the samples from radioactive decay. Therefore, both these samples were measured again by a thermal relaxation ("diffusivity") technique in which one end of the sample is bonded directly to the refrigerator. See Fig. 3(b). Current is supplied to a heater at the opposite end until an equilibrium is achieved, and then interrupted. The exponential temperature decay of the sample to the base temperature of the refrigerator is monitored. If τ is the 1/e decay time, and if the thermal conductivity κ is known, the specific heat C is computed from

$$C(\bar{T}) = \pi^2 \kappa(\bar{T}) \tau (4\ell^2)^{-1},$$

where ℓ is the length of the entire sample, and $\bar{T}$ is the average temperature across the sample with the heater on.

Since uncalibrated thermometry was used on the sample, there is some uncertainty in the average temperature since a thermal gradient is created by self heating. However, this gradient could be estimated since the thermal conductivity measurements utilized two precalibrated thermometers and revealed directly the self-heating gradient across the sample.[30] For the 270 h sample, this made a correction in $\bar{T}$ upward by about 1.5% for the lowest temperature point (0.19 K), and made negligible correction (<0.5%) for higher temperature points. For 2100 h, the correction was 8-2% for temperatures 0.17-0.29 K, and negligible above.

Uncertainty in the specific heat arises from ℓ, known to 1%, and τ, which was reproducible to $\approx$ 2%. The κ was previously determined to $\approx$ 4%, therefore C is uncertain by $\approx$7%. However, it was found, in comparison with the specific heat taken by the weak-link technique, that the diffusivity data were consistently high by 15-20%. Since this discrepancy was not a function of temperature, it has been ascribed to a change in geometry of the sample upon cryogenic cool-down; after cryogenic cycling cracks were observed in the samples near the epoxy bond. Therefore, for the plots and analysis the diffusivity data have been scaled downward by a factor of 0.80 and 0.85 for the 270 h and 2100 h samples, respectively, to agree with weak-link data taken at higher temperatures.

E. X-ray Characterization

The (100) x-ray reflections were measured for samples heat treated to 840°C. Samples 0 h, 3 h, and 27 h showed the

strong, narrow line characteristic of crystalline α-quartz. For the 270 h sample, the (100) reflection was nearly as narrow, but the angle was characteristic of β-quartz, a less dense crystalline phase which in unirradiated quartz exists only above 573°C. A transition from α- to β-quartz with irradiation has been noted previously.[31,32]

In comparison with x-ray work done by Wittels,[17] samples 3 h, 27 h, and 270 h should indeed retain crystallinity, and sample 2100 h should be amorphous. The measured mass density of 2100 h is identical with that of neutron-irradiated vitreous silica, which is amorphous.[33]

III. RESULTS AND DISCUSSION

A. Unirradiated Sample

The heat capacity and thermal conductivity of the 0 h sample were measured to calibrate the heat capacity addenda (Appendix A) and to provide a reference against which the irradiated samples could be compared. Unfortunately, the results for sample 0 h were more complicated than expected and must be discussed in detail.

Figure 4 shows the heat capacity of sample 0 h, mass 5.34 g, plus addenda. The data have been divided by T^3 to emphasize the departure from Debye phonon behavior. The rise in C/T^3 below 1 K is consistent with an estimate of the heat capacity of the addenda. Subtracting a fitted curve for the addenda leaves line A, which corresponds to a Debye heat capacity for phonons of average velocity $\bar{v} = 4.4 \times 10^5$ cm/s. This agrees with the value obtained from elastic constants.[11] Also shown in Fig. 4 is the heat capacity of sample 0 h, mass 5.12 g, after the 840°C anneal. There is an additional contribution to the heat capacity, this contribution having a temperature dependence of $\approx T^{0.5}$. The origin of this additional heat capacity is not known.

The thermal conductivity of sample 0 h is shown in Fig. 5. These data have been divided by T^3 to emphasize behavior different from a conductivity limited only by phonon scattering off the bulk boundaries of the sample (dashed line). Before anneal, κ/T^3 for 0 h shows a steep dip from 0.2-3 K. After an anneal to 840°C,

Figure 4. Heat capacity of sample 0 h (unirradiated) plus addenda, divided by T^3.

× Prior to heat treatment, mass of sample 5.34 g.

+ Following heat treatment to 840°C, mass of sample 5.12 g.

Line A is the heat capacity of the 5.34 g sample after subtraction of the fitted heat capacity contributed by the addenda. The inset illustrates the shape of the central colored region observed in the annealed 0 h sample, and in the irradiated 3 h and 27 h samples.

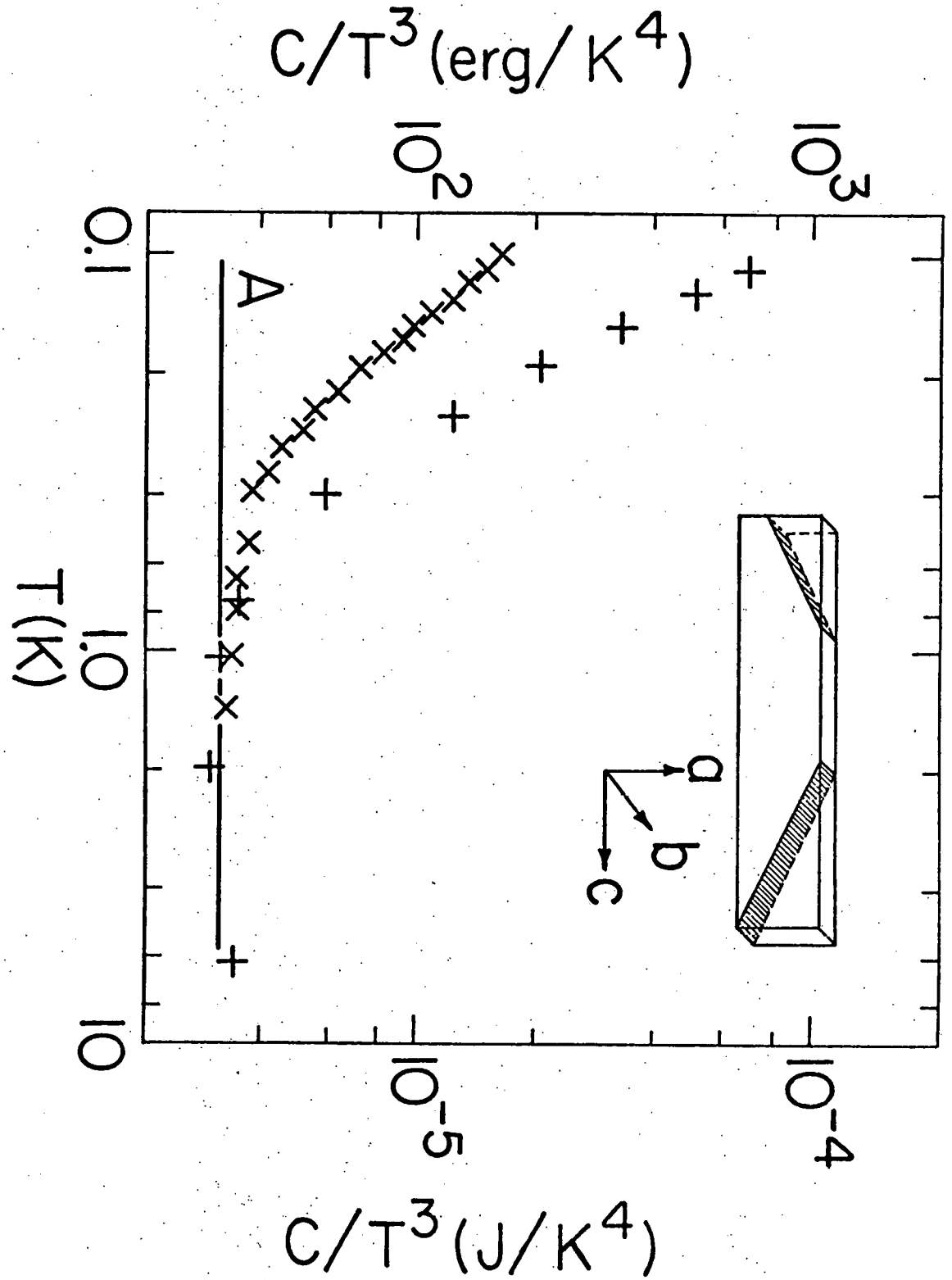
C/T³(erg/K⁴)
10²
10³
0.1
A
T(K)
1.0
10
10⁻⁵
10⁻⁴
C/T³(J/K⁴)
a
b
c

Figure 5. Thermal conductivity of unirradiated sample 0 h, divided by T^3 to emphasize departures from boundary scattering.

× Central region prior to heat treatment, 0.4 cm x 1.0 cm cross section.

+ Central, colored region after heat treatment to 840°C, 0.4 cm x 1.0 cm cross section.

◇ Region outside colored area after heat treatment to 840°C, 0.40 cm x 0.45 cm cross section.

The dashed line indicates κ/T^3 limited by boundary scattering for a cross section of 0.40 cm x 1.0 cm, not corrected for phonon focusing or finite sample length. Solid curves are discussed in the text.

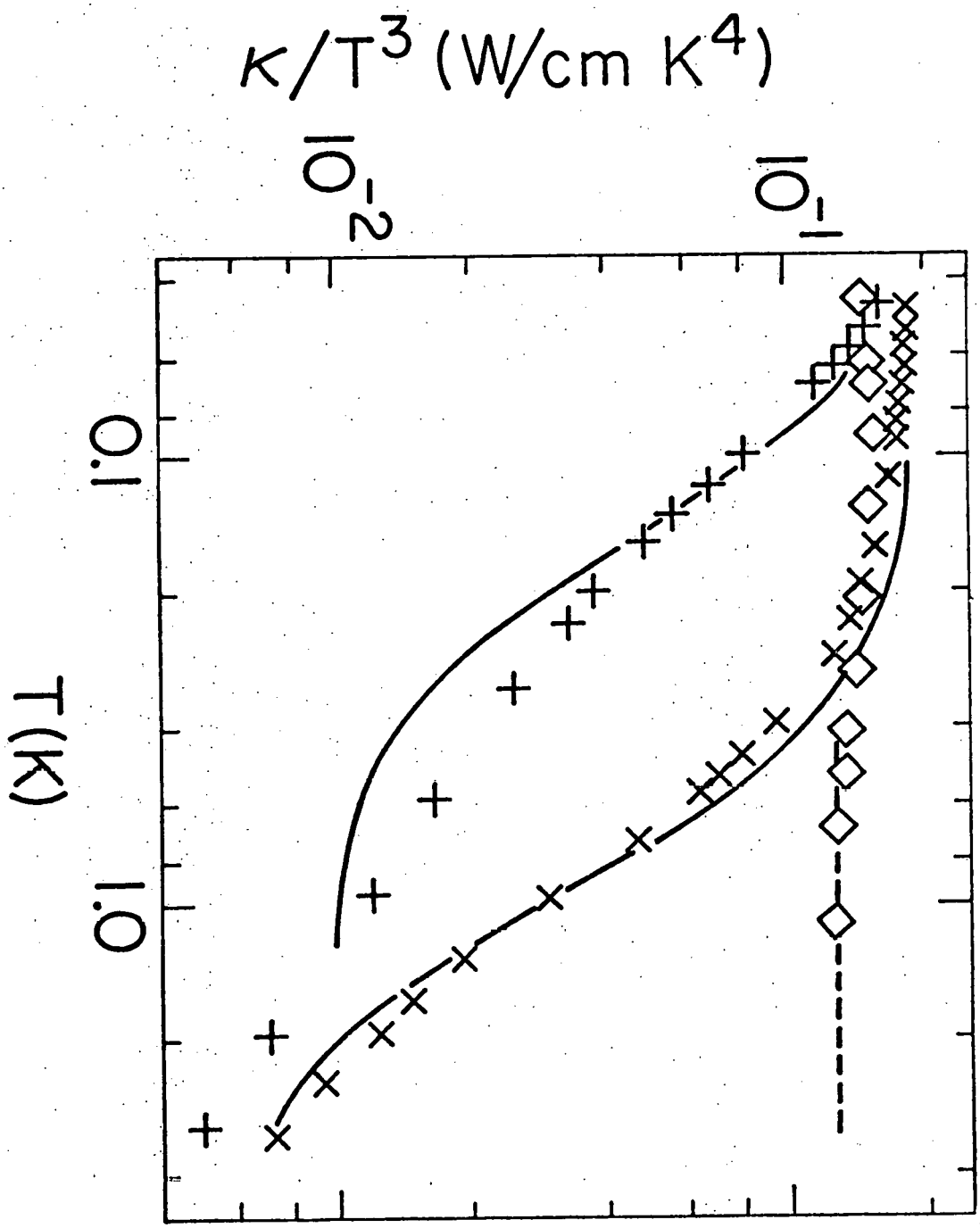
κ/T³ (W/cm K⁴)
O₂
O₁
T (K)
1.0
0.1

sample 0 h revealed a central region identical in shape to that of 3 h and 27 h, and the region appeared blue to scattered light and brown to transmitted light. The thermal conductivity (divided by T^3) in the central region dropped over the temperature range 0.04-3 K, as shown. (The κ of the unannealed 0 h sample was also measured in the central region, although the region was not visible at the time.) The conductivity of the annealed outer region shows the expected T^3 dependence with a magnitude predicted approximately by boundary scattering.

The optical appearance of the annealed central region is suggestive of Rayleigh scattering of light off inclusions within the crystal, inclusions of diameters < 3000 Å. Such inclusions would also scatter phonons of similar wavelength, thereby causing a dip in κ/T^3 for temperatures ~ 0.1 K.[34] If a density N of spherical inclusions is assumed, all inclusions having the same radius r, the phonon mean free path ℓ as a function of frequency ω would be given by $\ell = (\ell_B^{-1} + \ell_I^{-1})^{-1}$, where ℓ_B is from boundary scattering[35] and $\ell_I = (N\pi r^2)^{-1}$ if the phonon wavelength $\lambda \lesssim r$, and[36] $\ell_I = 9(4\pi r^2 N)^{-1}(\bar{v}/r\omega)^4$ if $\lambda \gtrsim r$. The calculation of a thermal conductivity from the above mean free path is described in Appendix B. The fitted curve through the data in Fig. 5 for the sample before heat treatment gives $r \approx 80$ Å and $N \approx 2 \times 10^{13}$ cm^{-3}, and for the annealed sample $r \approx 460$ Å and $N \approx 3 \times 10^{11}$ cm^{-3}. If the inclusions were Ca colloids, the foregoing values would imply 20 ppm (wt.) and 70 ppm (wt.) Ca, respectively. Given the uncertainty in the impurity measurements and that a perfect con-

densation would not be needed to produce an "inclusion," impurity colloids could account for the thermal conductivity. Rayleigh-like phonon scattering from metallic colloids in a dielectric crystal has been reported previously.[37] As noted, the thermal conductivity in the annealed outer region showed no scattering from inclusions; yet the measured impurity content was similar to the central region. Therefore some growth defect might be responsible for an initial impurity condensation in the central region.

B. Irradiated Samples

Figure 6 shows the thermal conductivity of the irradiated samples, measured in the central region (however, 270 h and 2100 h displayed no colored central region). The conductivity decreases with irradiation except in the case of the 2100 h sample, which has a larger κ than sample 270 h. Figure 7 shows the conductivity of the samples annealed to 840°C. Sample 2100 h was only annealed at 370°C, and no change in conductivity was observed. The conductivity of sample 3 h dropped for $T \lesssim 1$ K, but increased for $T \gtrsim 1$ K, matching closely the κ of 0 h annealed above 1 K. Sample 27 h showed a similar increase for temperatures above 0.5 K, but no change at lower temperature. Sample 270 h also showed no change below ≈ 0.5 K. Although the "plateau" will not be studied in detail here, it is noted that the plateau in κ for 270 h dropped by a factor 2.3 upon the 840°C anneal. However, the most irradiated sample of Berman increased[15] in conductivity in this temperature range, as did our less irradiated samples.

Figure 6. Thermal conductivities of irradiated samples.

△ 3 h

○ 27 h

□ 270 h

▽ 2100 h

For reference:

A Unirradiated sample 0 h from Fig. 5.

B Vitreous silica (Ref. 14).

C Neutron-irradiated vitreous silica (Ref. 14).

D, E, F Data on neutron-irradiated quartz from Ref. 15.

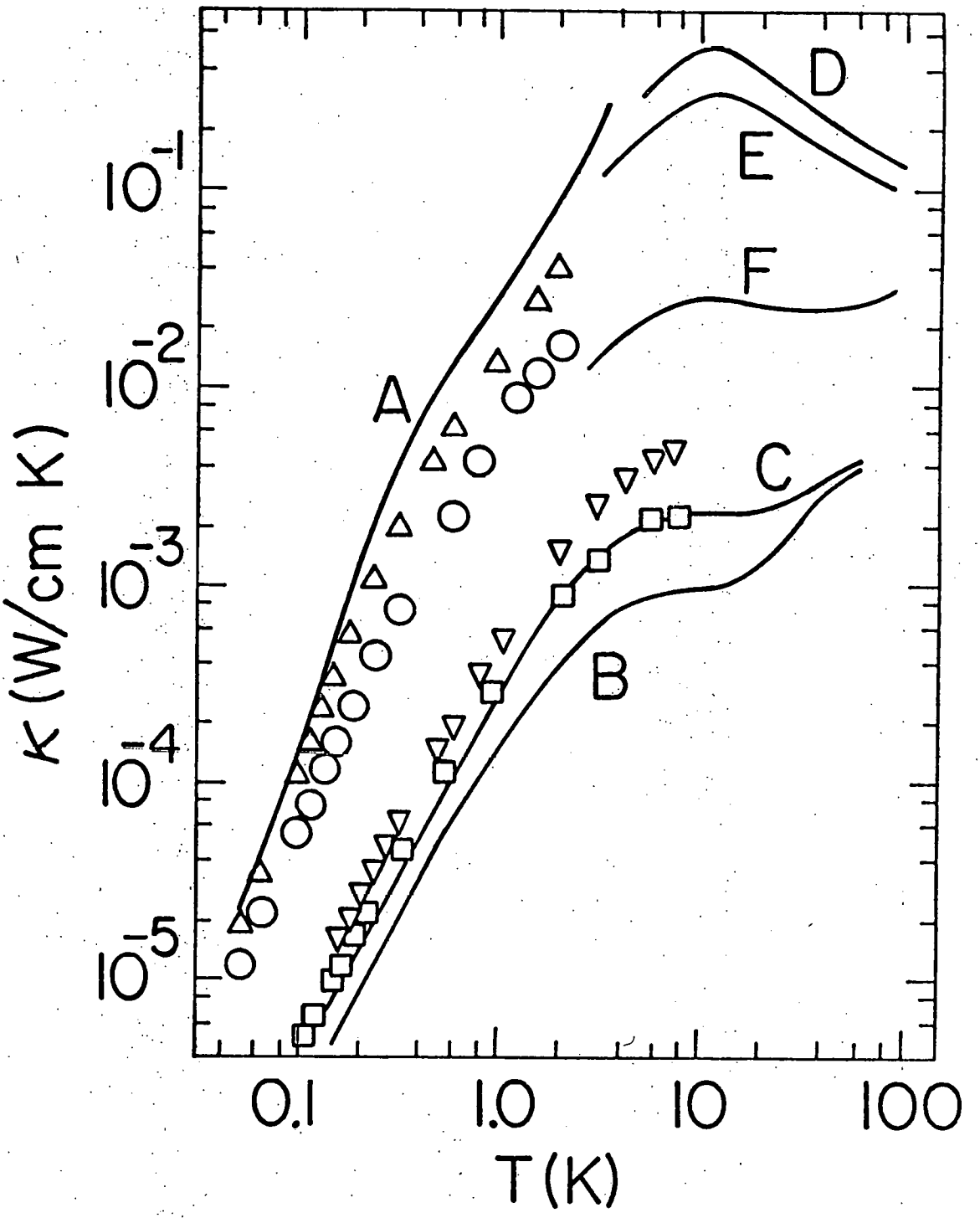
D
E
F
A
C
B
10^{-1}
10^{-2}
10^{-3}
10^{-4}
10^{-5}
κ (W/cm K)
0.1
1.0
10
100
T(K)

Figure 7. Thermal conductivity of irradiated samples after heat treatment to 840°C. Same scale as Fig. 6.

△ 3 h

○ 27 h

□ 270 h

For reference:

A Heat treated, unirradiated sample 0 h from Fig. 5.

B, C Same as in Fig. 6.

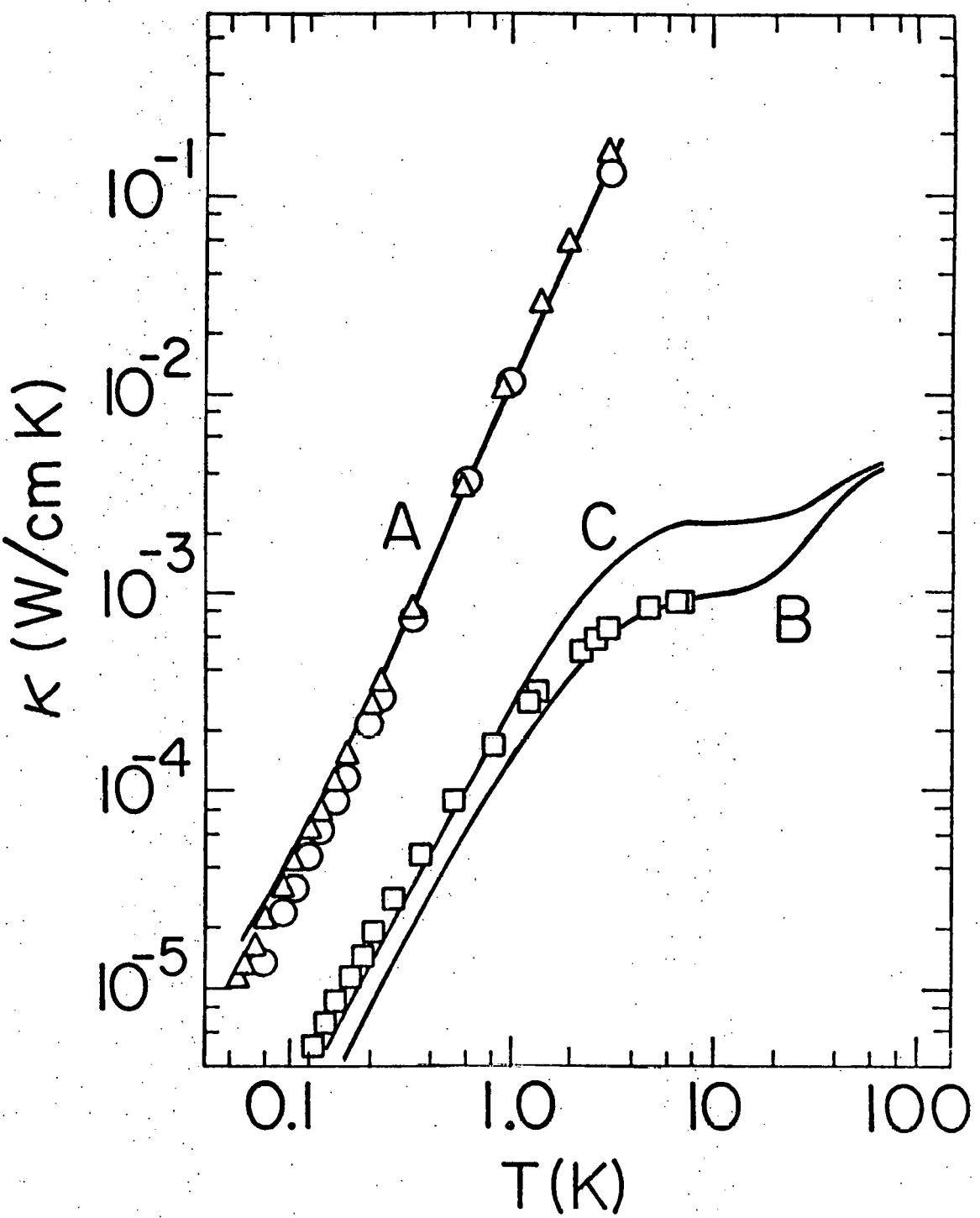
10^{-1}
10^{-2}
10^{-3}
10^{-4}
10^{-5}
κ (W/cm K)
A
C
B
0.1
1.0
10
100
T(K)

The specific heats of the samples are shown in Figs. 8 and 9. Addenda contributions have been subtracted. A prominent peak occurs near 1 K and increases in magnitude with irradiation, except for sample 2100 h. Similarly, a contribution for $T \lesssim 0.5$ K increases with irradiation, except for 2100 h.

An anneal at 370°C had the following effects on specific heat: For 2100 h, the peak was reduced by at least an order of magnitude; at lower temperatures the specific heat did not change. For 270 h, an anneal at 370°C (for only 1 h) produced no change over the measured temperature range (0.2-1.3 K). For 3 h, the 1 K peak did not change, but for lower temperatures, 0.2-0.4 K, the specific heat dropped smoothly by 10-50%. Sample 27 h was not annealed at 370°C.

The specific heat of samples annealed to 840°C is shown in Fig. 10. The peak near 1 K is sharply reduced in all cases. The specific heat below 0.4 K is nearly unchanged for 270 h, reduced by a factor of three for 27 h, and increased by ≈35% for sample 3 h. The specific heat of the 3 h sample is now nearly identical to the specific heat of the annealed 0 h sample.

We thus see a complicated set of changes occurring with irradiation and heat treatment. In order to discover evidence for glass-like excitations we shall rely first on the thermal conductivity, since samples 270 h and 2100 h show distinct glass-like behavior here, and then ask whether there is corresponding evidence in the specific heat. Therein lies the first problem: there are "extraneous" excitations in the specific heat. Additionally,

Figure 8. Specific heat of irradiated samples, divided by T^3 to emphasize departure from Debye behavior.

△ 3 h

○ 27 h

□ 270 h

For reference:

A Debye phonon contribution from Fig. 4.

B Vitreous silica (Ref. 14).

C Calculated for a two-level Schottky peak plus phonon contribution.

[1]The specific heat of neutron-irradiated vitreous silica (Ref. 14) lies about 30% below curve B.

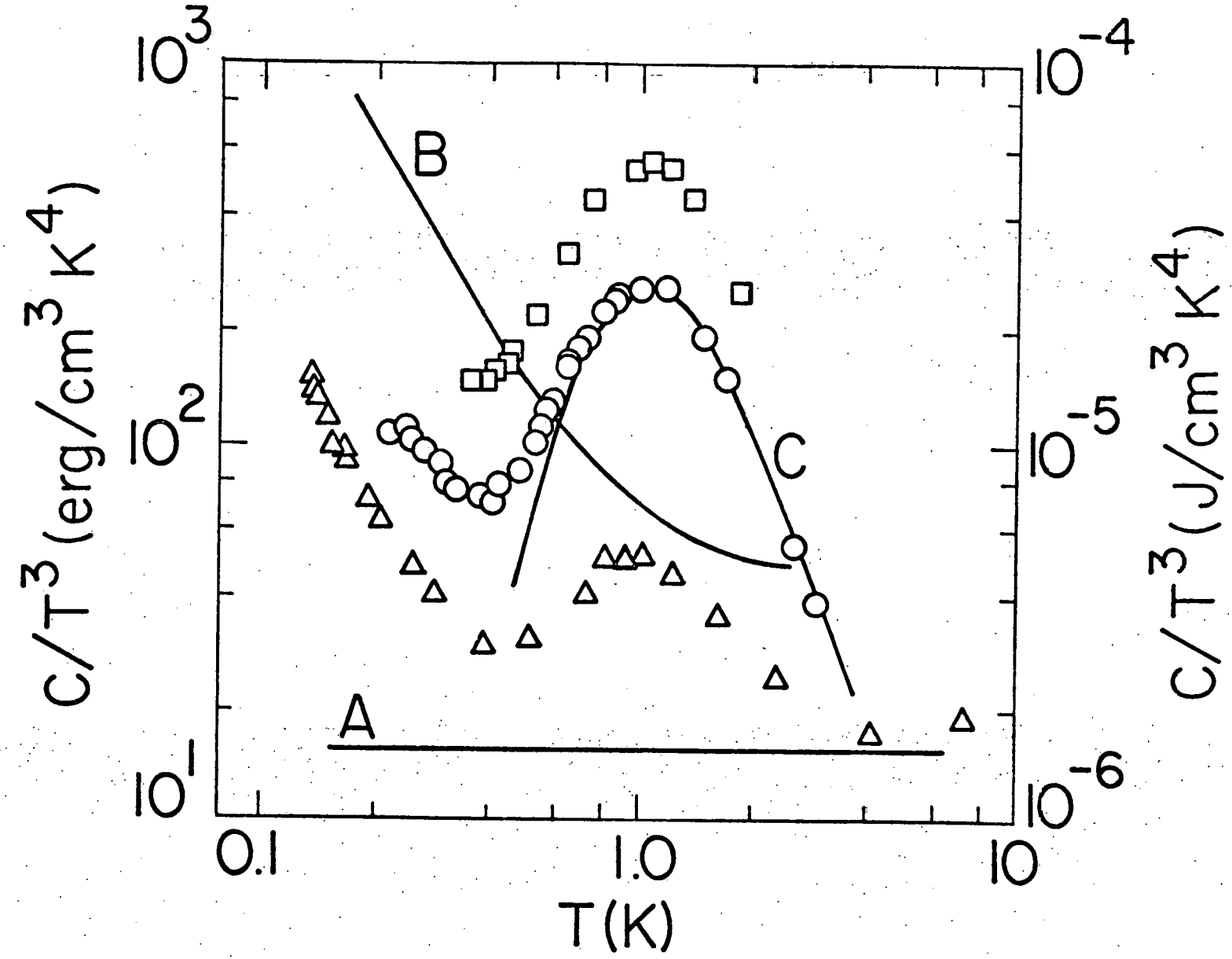
10^3
10^2
10^1
10^{-4}
10^{-5}
10^{-6}
C/T^3 (erg/cm^3 K^4)
C/T^3 (J/cm^3 K^4)
B
C
A
0.1
1.0
10
T(K)

Figure 9. Specific heat, divided by T^3, for irradiated sample 2100 h. Same scale as Fig. 8.

▽ Before heat treatment.

▼ Following heat treatment at 370°C.

Curves A and B same as in Fig. 8. The curve through the data was calculated from the measured thermal conductivity of this sample as explained in the text.

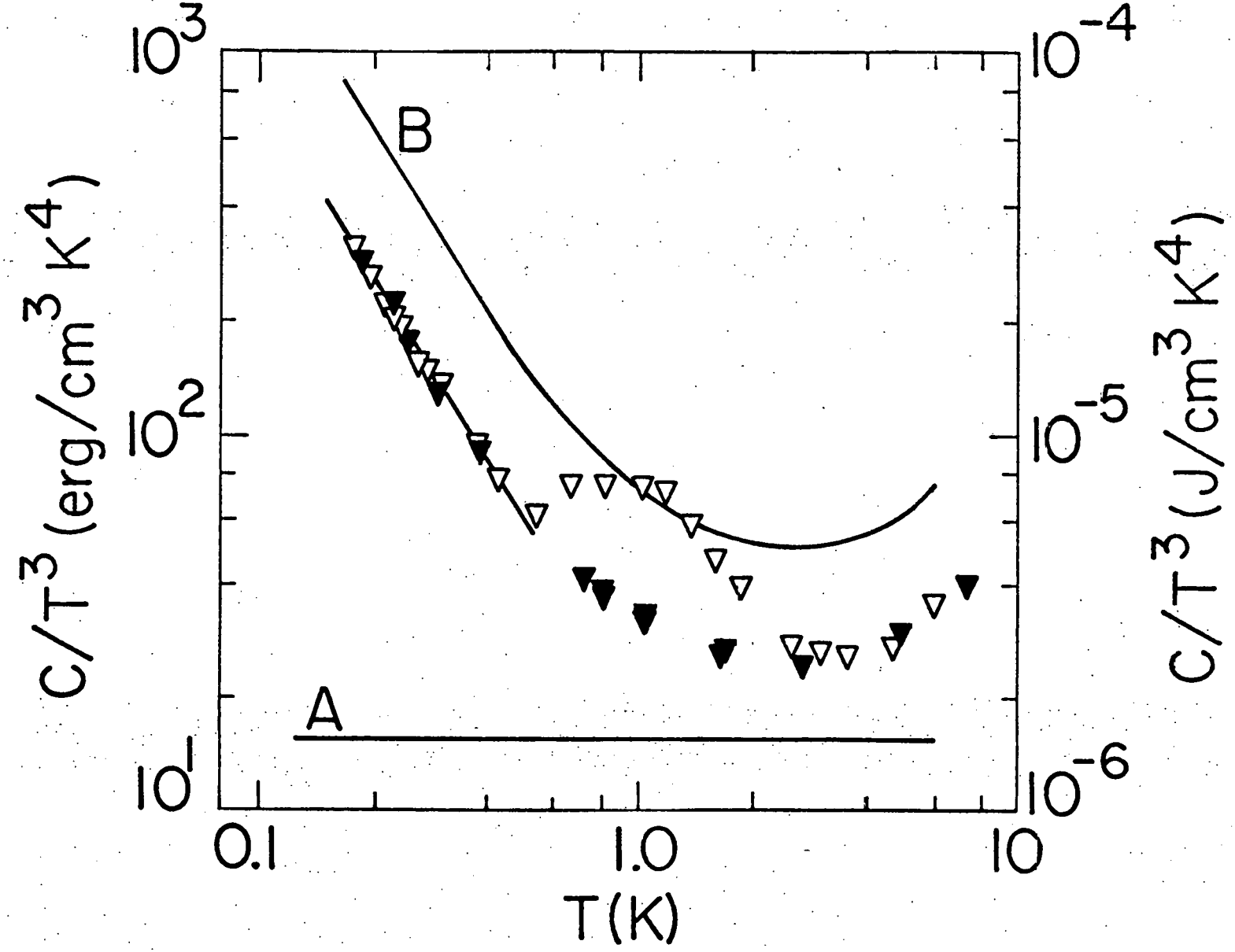
10^3
10^2
10^1
10^{-4}
10^{-5}
10^{-6}
B
A
0.1
1.0
10
T(K)
C/T^3 (erg/cm^3 K^4)
C/T^3 (J/cm^3 K^4)

Figure 10. Specific heat, divided by T^3, of neutron-irradiated samples heat treated to 840°C. Same scale as Figs. 8 and 9.

▲ 3 h

● 27 h

■ 270 h

For reference:

+ Unirradiated sample 0 h after heat treatment to 840°C, from Fig. 4 (addenda contribution subtracted).

A Debye phonon contribution.

The two lines near the 27 h and 270 h data were calculated from the measured conductivities of the respective samples as explained in the text.

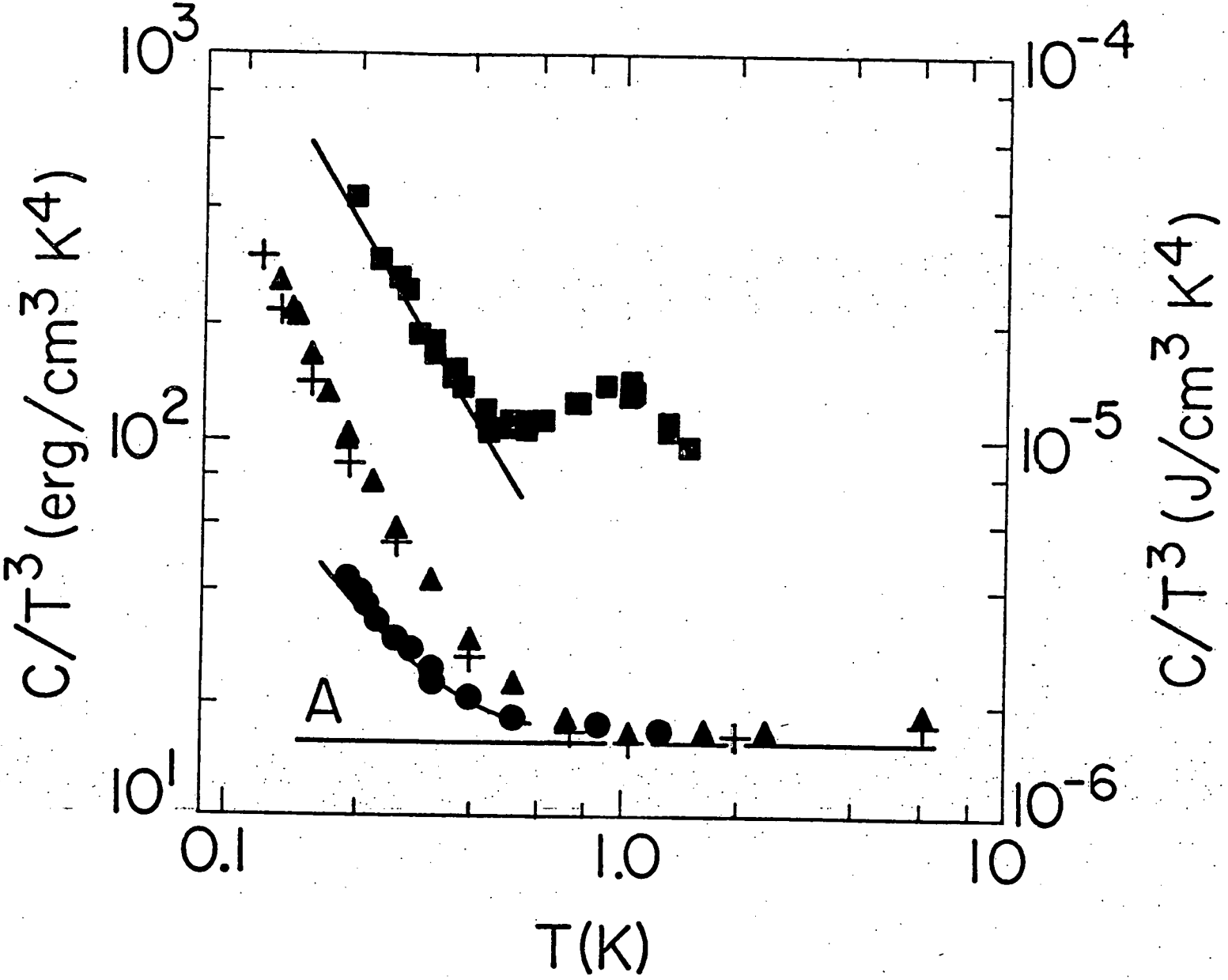
10^3
10^2
10^1
C/T^3 (erg/cm^3 K^4)
10^{-4}
10^{-5}
10^{-6}
C/T^3 (J/cm^3 K^4)
0.1
1.0
10
T(K)
A

it must be determined whether these excitations have a significant effect on the thermal conductivity. The motivation for annealing the samples was to attempt to remove these other excitations without also removing glass-like excitations. It will be shown this was a successful procedure, except for the 3 h sample, where an additional set of excitations was produced by annealing. Sample 27 h, the most intermediate of the samples in some respect, will require the most delicate discussion. In the discussion following, we first treat the extraneous excitations evidenced in the specific heat, comparing these with similar excitations noted in the literature. Secondly, the thermal conductivity will be considered for evidence of glass-like states and then compared with the specific heat of annealed samples. Lastly, the character of the neutron damage in the samples will be considered and the implications of the results for the strain broadening model for the density of glass-like states, n(E), will be discussed.

C. Discussion

The large peak in C/T^3 at ≈ 1 K observed in the irradiated samples is fitted extremely well by a Schottky two-level specific heat[38] having an energy splitting 5.3 K (see Fig. 8). These two-level excitations cannot be shown to be a sharp energy distribution of glass-like excitations since there is no definitive phonon scattering. It is true that the thermal conductivities of samples 3 h and 27 h show an increase above 1 K upon the 840°C anneal, an anneal which reduced the Schottky peaks by a factor $\gtrsim 100$. However, as seen from Fig. 6, the conductivity of the

unannealed 3 h or 27 h sample is smaller than that of the 0 h sample by a constant factor for temperatures 0.5-2 K. In the same temperature range the magnitude of the Schottky specific heat increases by ≈200. This would argue against[39] resonant scattering by the excitations. Additionally, it is noted that for sample 270 h the conductivity decreased above 1 K upon 840°C anneal, where the Schottky peak was reduced by a factor of 5.

A Schottky peak with approximately the same splitting has been seen in the specific heat of a commercial species of vitreous silica;[40,41] again, with no evidence of phonon scattering in the thermal conductivity. The peak was reduced upon electron irradiation[40] or heat treatment[41] at 1300°C. Furthermore, the Schottky excitations reported in Refs. 40 and 41 could not be associated with a particular impurity, although there was sufficient impurity present to account for the observed magnitude of the peak. We have evidence that the Schottky anomaly in our samples is not due to impurities. The magnitude of the peak in sample 270 h implies a density of Schottky excitations of 2.7×10^{19} cm^{-3}, a factor ≈500 larger than the known impurity level. Therefore, these excitations may involve some defect of the SiO_2 system. A summary of the Schottky densities and the effects of anneal are given in Table 2.

Another low-energy excitation expected in neutron-irradiated quartz is that created by the γ radiation present in the reactor. Chaussy, et al.,[42] observe an anomalous specific heat linear in temperature for $T < 1$ K in γ-irradiated quartz. They ascribe this broad spectrum of excitations to activated Al states, which are

TABLE 2. Number of Schottky excitations (per cm^3) contributing to the peak in C/T^3 at 1 K following irradiation and following heat treatment at 370°C and 840°C.

Sample:	0 h	3 h	27 h	270 h	2100 h
after irradiation	0	2.0×10^{18}	1.2×10^{19}	2.7×10^{19}	2.4×10^{18}
after 370°C anneal	0	2.0×10^{18}	-	2.7×10^{19}	$< 10^{17}$
after 840°C anneal	0	$< 4 \times 10^{16}$	$< 4 \times 10^{16}$	5.6×10^{18}	-

known[43] to anneal out at a temperature of 350°C. The purpose of our 370°C anneal was to remove these excitations. Additionally, in Ref. 42, no thermal scattering could be detected from the states. It is seen that our sample 27 h before anneal shows an approximately linear specific heat for $T \lesssim 0.4$ K (Fig. 8). It will be shown later that a specific heat expected from glass-like excitations is much less than this. Using a width of 6 K for the spectrum of the Al excitations as in Ref. 42, the magnitude of the observed excess specific heat (above the phonon contribution) would imply a concentration of ≈ 5 ppm (wt.) Al, close to the measured abundance value. Our sample received $\sim 3 \times 10^7$ R; Chaussy found a similarly large Al activation by a like dose. After sample 27 h was annealed to 840°C, the excess specific heat did drop significantly (factor of 3), resting close to a magnitude expected from glass-like excitations (to be shown). Sample 3 h also experienced a drop in specific heat for $T < 0.5$ K upon anneal at 370°C. This drop could be accounted for by a 1 ppm (wt.) initial Al activation. A similarly smaller activation was also observed at lower doses in the Chaussy samples. We note further that our samples 270 h and 2100 h showed no evidence of these excitations; the low-temperature ($T \lesssim 0.5$ K) specific heat showed no change with anneal. In Ref. 42, a specific crystalline environment (α-quartz) was used to give a microscopic description of the Al excitations, and with our samples 270 h and 2100 h there occurs significant deviation from the α-quartz structure. Hence the Al excitations may not exist in these samples.

In summary we note simply that an anneal to 840°C eliminates or sharply reduces the Schottky excitations contributing a peak near 1 K, and the anneal should also eliminate the γ-induced excitations observed at lower temperature.

Unfortunately, such an anneal creates a rather broad spectrum of excitations in samples 0 h and 3 h below 1 K (but apparently not in the more irradiated samples). These anneal-induced excitations, like the Schottky and Al excitations, might not appear in the thermal conductivity: For annealed sample 0 h, the excess specific heat increases as $\approx T^{0.5}$ for temperatures 0.1-0.5 K; however, the additional thermal resistance brought about by the anneal has a varying temperature dependence from $\approx T^{0.9}$ at 0.1 K to $\approx T^{2.5}$ at 0.5 K (see Fig. 5). An energy-dependent coupling between the excitations and the lattice could bring about the observed scattering. However, we have preferred a simpler picture where the phonon scattering is from inclusions. An argument against the latter might be that the fit to the thermal conductivity is not impressively good for the annealed 0 h sample (Fig. 5); however, a better fit could be made by assuming a distribution of inclusion sizes.

The question is now asked, is there evidence for glass-like excitations in the irradiated samples, and what is the nature of their energy spectrum? Samples 270 h and 2100 h will be treated first. These samples displayed the following thermal conductivities, in W cm^{-1} K^{-1}, for $T \lesssim 0.5$ K:[44]

$$\kappa_{270\ h} = 3.8 \times 10^{-4}\ T^{1.96}$$

$$\kappa_{\substack{270\ h \\ ann.\ 840^{\circ}C}} = 3.3 \times 10^{-4}\ T^{1.85}$$

$$\kappa_{2100\ h} = 4.7 \times 10^{-4}\ T^{1.87}$$

A thermal conductivity varying as T^s, $s \approx 2$, is characteristic of a glass and indicative of a broad, energy-insensitive spectrum of glass-like excitations. In particular, $s \approx 1.8$ for vitreous silica.[14]

The tunneling states model makes the following connection between the excess specific heat (i.e., that above the phonon contribution) and the thermal conductivity. Let the density of glass-like excitations per unit energy per unit volume be denoted, as before, $n(E)$, where E is the energy splitting of these presumably two-level excitations. If $n(E) \propto E^m$ (where m typically is ≈ 0.1 for glasses), then[14] $\kappa \propto \gamma^{-2}\ T^{2-m}$ and $C \propto T^{1+m}$. The γ is the coupling constant[14,19] between the glass-like excitations and the lattice phonons. To avoid constants of proportionality, the quantities are normalized to vitreous silica:

$$C_x = C_g \frac{\kappa_g}{\kappa_x}\left[\frac{\gamma_x}{\gamma_g}\right]^2 \qquad (1)$$

where C_g and κ_g refer[45] to the glass vitreous silica, and C_x and κ_x to the irradiated sample.[46] Under the assumption $\gamma_x = \gamma_g$, C_x is plotted near the respective data in Fig. 10. The Debye phonon contribution has been added. For sample 270 h, κ_x of the annealed sample has been used to compare with the annealed specific heat. The agreement is excellent and is within the margin of measurement uncertainty. Therefore, the identicality of the coupling constants among vitreous silica, sample 270 h, and sample 2100 h is demonstrated

to within 7%.

For samples 3 h and 27 h, the appropriate thermal conductivity to use for κ_x in Eq. 1 is that conductivity limited only by the excitations created by the neutron irradiation. For these two samples, there is a significant contribution to the thermal resistance from bulk boundary scattering and additionally from the "inclusions." The 0 h sample, since it has the same bulk cross section as 3 h and 27 h and presumably an identical inclusion composition, calibrates these resistances. Therefore they can be "removed" from an irradiated sample by subtracting the inverse conductivity of 0 h:

$$\kappa_x^{-1} = \kappa^{-1} - \kappa_{0\ h}^{-1} \qquad (2)$$

where κ is the measured conductivity of an irradiated sample. It has been mentioned that comparison of thermal conductivities to annealed specific heats may be necessary. In that case Eq. 2 should refer to the conductivities of annealed samples. For sample 3 h this gives, for $T < 0.4$ K (Fig. 11),

$$\kappa_{x\ 3\ h} = 7.7 \times 10^{-2}\ T^{2.46}\ \ \mathrm{W\ cm^{-1}\ K^{-1}}$$

If Eq. 1 is used, the above conductivity predicts an excess specific heat a factor $\approx$20 less than observed (the predicted curve, not plotted, falls close above line A in Fig. 10). However, it is clear from Fig. 10 that the specific heat of the annealed 3 h sample is completely dominated by the unidentified excitations also observed in sample 0 h after anneal. Thus, no claim for the presence of glass-like excitations in sample 3 h can be made.[47]

For sample 27 h, there is reason to believe Eq. 2 will not be valid for annealed sample conductivities. It is noted that the

Figure 11. Thermal conductivity K_x of samples before and after heat treatment to 840°C. The K_x is the inverse thermal resistance of an irradiated sample after subtraction of the thermal resistance of the unirradiated sample 0 h, see Eq. 2 in text.

△ 3 h before heat treatment

▲ 3 h after heat treatment

○ 27 h before heat treatment

● 27 h after heat treatment

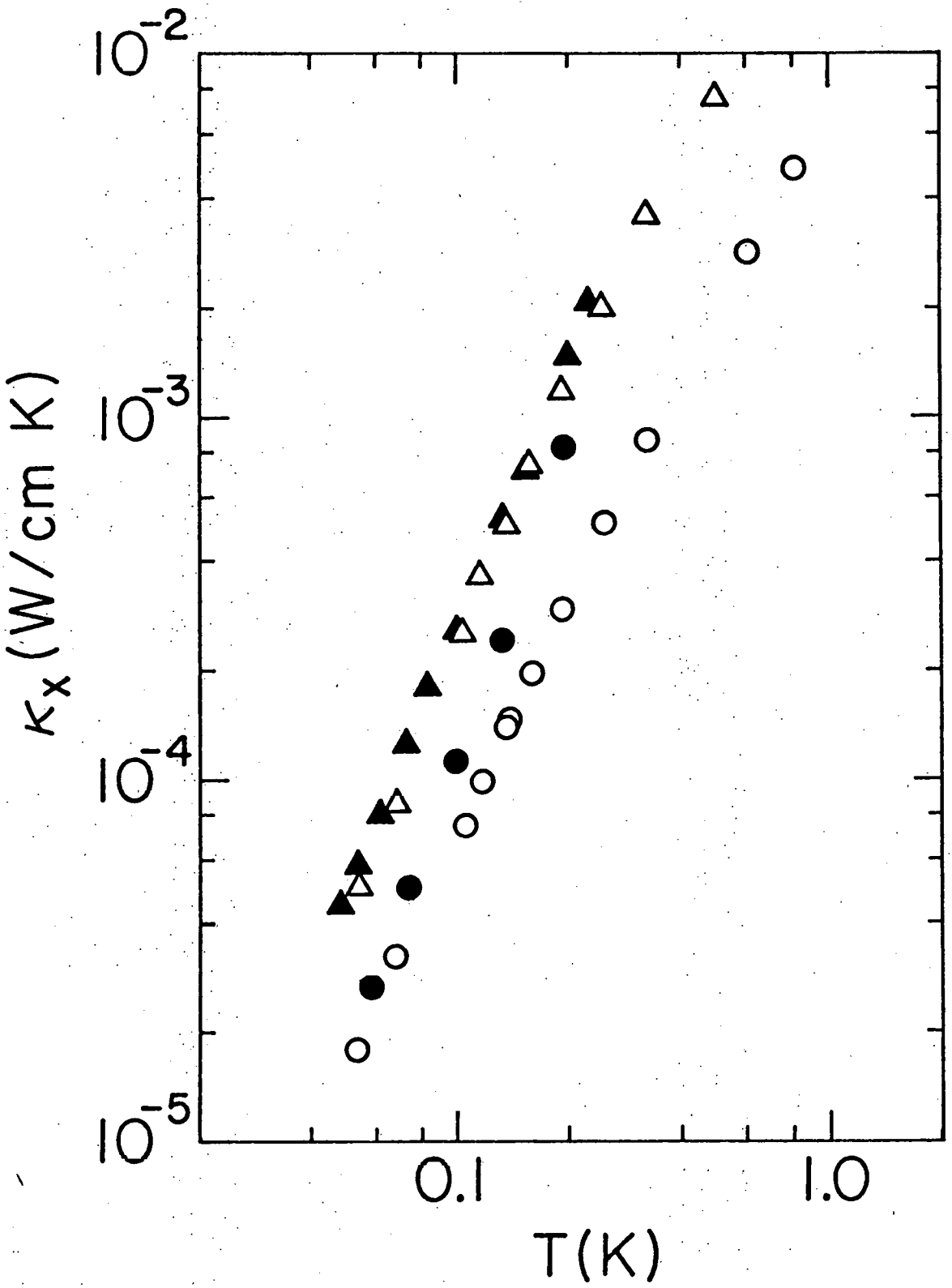
10^{-2}
10^{-3}
10^{-4}
10^{-5}
κ_x (W/cm K)
0.1
1.0
T(K)

840°C anneal dropped the conductivities of samples 0 h and 3 h by a similar factor for $T \lesssim 0.5$ K (Figs. 6 and 7); however, the anneal did not produce a change in the 27 h conductivity ($T \lesssim 0.5$ K). It is plausible that the scattering associated with inclusions is not scaling similarly upon anneal for sample 27 h as for sample 0 h; hence the calibration of the inclusion scattering in Eq. 2 fails. However, it may be valid to use Eq. 2 with the unannealed conductivities to discover a κ_x that may be compared with the annealed specific heat. This is recommended by several facts. (1) The excess excitations, namely Schottky and Al, present in the unannealed 27 h but not in 0 h, did not appear to affect thermal conductivity. (2) The κ_x for samples "on either side" of 27 h, i.e., 3 h and 270 h, did not change (for $T \lesssim 0.4$ K) upon anneal, see Fig. 11 and Figs. 6 and 7. (3) At the lowest temperatures, where inclusion scattering diminishes and bulk boundary scattering begins to predominate (see Fig. 5), the κ_x as computed from annealed 27 h and annealed 0 h approaches asymptotically that for the unannealed case, see Fig. 11. Therefore, using the unannealed sample conductivities, Eq. 2 gives

$$\kappa_{x\ 27\ h} = 9.4 \times 10^{-3}\ T^{2.13}\ \ \mathrm{W\ cm^{-1}\ K^{-1}}$$

for $T \lesssim 0.4$ K. The temperature dependence is suggestive of the presence of a broad spectrum of glass-like excitations. Using the above κ_x, Eq. 1 predicts the line near the annealed 27 h specific heat data in Fig. 10 (phonon contribution has been added). Agreement is good, and the data lie $\approx$10% above the predicted line. However, it is not known what contribution any possible remnant excitations similar to those found in the annealed 0 h and 3 h samples might

make to the data.

There is a further complicating factor with sample 27 h. The thermal conductivity of the annealed outer region was measured and κ_x[48] was a factor ≈ 4 higher than in the central region.[49] Therefore, the predicted excess specific heat for sample 27 h, which by volume is $\approx 70\%$ central region and $\approx 30\%$ outer region, should be lowered by a factor 0.8. With this adjustment, the predicted excess specific heat is $\approx 65\%$ of that measured. If it is assumed that the entire excess specific heat is due to glass-like excitations, the coupling constant γ in the 27 h sample would be $\approx 17\%$ smaller than in vitreous silica. Of course, as mentioned above, there might be contributions to the specific heat from other excitations.

As posited in Chapter 1, the microscopic nature of fast-neutron damage in crystals is not well known. Nevertheless, estimates have been made of the amount of damage present in the irradiated samples. In Table 3, row A gives the number of "damage clusters" in each sample. This number is calculated assuming a damage region of[23] 10^4 atoms is produced by each fast-neutron collision. The number of collisions per cm^3 is $N\sigma\Phi$, where N is the atomic density, 8×10^{22} cm^{-3}, σ is the scattering cross section,[23] 3.5×10^{24} cm^2, and the dose Φ is taken from Table 1 in the 0.1 MeV - ∞ range. Row B of Table 3 lists the fractional volume of the total damage and row C the number of atoms in the total damaged volume. According to row B, sample 270 h is the first sample estimated to be "completely" damaged. The sample also exhibited the lowest thermal conductivity and largest specific heat of the samples; sample 2100 h reversed

TABLE 3. Comparison of neutron-irradiated quartz samples. See text for details of estimates.

Sample:	3 h	27 h	270 h	2100 h
(A) radiation induced clusters per cm^3	8.1×10^{16}	7.6×10^{17}	7.3×10^{18}	5.9×10^{19}
(B) fraction of sample damaged	≈0.01	≈0.1	≈1.0	1.0
(C) total number of displaced atoms in damaged volume, per cm^3	8×10^{20}	8×10^{21}	7×10^{22}	(6×10^{23})
(D) ratio of glass-like excitation density compared to vitreous silica	(≈0.005)	0.024	0.53	0.39
(E) ratio of glass-like excitation density compared to neutron-irradiated vitreous silica	(≈0.007)	0.031	0.69	0.51
(F) total number of glass-like excitations of energy < 1 K, per cm^3	4.3×10^{14}	2.4×10^{15}	5.4×10^{16}	3.9×10^{16}

this trend. Saturation or reversal of other properties[33,50] in neutron-irradiated quartz has been reported near the 3×10^{19} cm^{-2} fast-neutron dose.

A summary of the densities of glass-like excitations observed in the samples is given in rows D, E, and F. Row D gives the fraction of glass-like excitations in neutron-irradiated quartz compared to vitreous silica; in row E, compared to neutron-irradiated vitreous silica. The fraction was calculated from the ratio of the respective thermal conductivities [51] (central region κ_x was used for samples 3 h and 27 h). Sample 3 h is included, although no independent evidence for glass-like excitations was found in this sample. It is noted for sample 270 h that crystalline, neutron-irradiated quartz can attain 70% the density of glass-like excitations of amorphous, neutron-irradiated vitreous silica. In row F, the number of glass-like excitations per cm^3 with energy splitting less than 1 K is calculated.[52] These densities allow only one excitation for every ≈ 200 damage clusters. It is not known how far the energy spectrum of glass-like excitations extends above 1 K since other, not independently characterized processes enter into the specific heat and thermal conductivity of glasses.[53] However, if the spectrum extends to ≈ 40 K, as has been suggested for vitreous silica,[14] and with an energy dependence similar to vitreous silica,[14] the values in row F would be increased by a factor of 2000. Such a density would put ~ 10 glass-like excitations in each damage cluster for samples 3 h, 27 h, and 270 h. It should be noted that the density of glass-like excitations observed in the samples is not consistent with a

conjecture that local vitrification in the sample occurs upon irradiation, i.e., that each damage cluster is a pocket ("thermal spike"[33]) of vitrified material. For sample 270 h, ≈50% by volume glass would be required, inconsistent with the measured density. The invalidity of the thermal-spike picture for quartz has been stated previously.[33]

We now consider the bearing of the results on the strain broadening model discussed in Chapter I. It was stated that for a concentration of glass-like excitations (assumed to be tunneling systems) a factor ~10 smaller than found in vitreous silica, interaction strain broadening would no longer hold and, conceivably, sharp peaks in the density of states, n(E), could exist. No such sharp distributions of glass-like excitations were detected in the present samples, at least over the energy range ≈0.1-5 K. Indeed, the results for sample 27 h suggest a broad spectrum of glass-like excitations persists even at a dilution of 1/40 compared to vitreous silica. One might therefore believe some other mechanism is responsible for the broad n(E) observed in glasses. However, Table 3 shows that the fraction of glass-like excitations compared to vitreous silica is roughly equal to the fraction of the sample damaged (rows B and D). This suggests that the excitations are clustered with local densities equivalent to that in vitreous silica. Hence strain interactions could still be important, assuming that there were in fact many excitations present in each cluster. It is therefore seen that the form of n(E) above 1 K has critical bearing on this question; the aforementioned factor of 2000 is necessary to produce even just 10 excitations per cluster. Until it is discovered definitively how

to measure n(E) for E > 1 K, or until the damage regions can be probed locally for glass-like excitations, it appears that interaction strain broadening is still a viable model for the universal n(E) observed in glasses.

IV. SUMMARY

The following is a summary of the major experimental results. It has been shown that neutron-irradiated quartz exhibits a low-temperature specific heat and thermal conductivity characteristic of glasses. In particular, the density of "glass-like" excitations giving rise to these thermal properties may attain 50% the density of that in vitreous silica, yet the irradiated quartz still retain long range atomic order. For a less irradiated sample, a density of glass-like excitations $\approx 2.5\%$ that in vitreous silica may be produced, with an energy spectrum similar to that in vitreous silica for the energy range 0.1-1 K. The density of glass-like excitations in the irradiated quartz increases with irradiation up to a fast-neutron dose $\approx 3 \times 10^{19}$ cm^{-2}, and is subsequently reduced for a dose $\approx 2 \times 10^{20}$ cm^{-2}. The density of glass-like excitations is not changed upon a brief anneal to 840°C.

In addition to glass-like excitations, neutron-irradiated quartz exhibits in the specific heat a two-level Schottky anomaly with splitting 5.3 K. The magnitude of this anomaly increases with irradiation up to a fast-neutron dose $\approx 3 \times 10^{19}$ cm^{-2}, and is subsequently reduced for a dose $\approx 2 \times 10^{20}$ cm^{-2}. A brief anneal to 840°C sharply reduces the magnitude of the anomaly.

APPENDIX A

ADDENDA HEAT CAPACITY

It is important to know the heat capacity of the addenda in the weak-link specific heat experiments since, for the less-irradiated samples, this is a significant contribution to the total heat capacity for $T < 1$ K. First, we estimate the expected heat capacity of the addenda for $T \lesssim 4$ K:

(1) Thermometer composed of

0.0025 g carbon:[54]	$0.05T + 0.25T^3$ erg/K
0.003 g Mylar:[1]	$0.14T + 0.88T^3$
0.006 g epoxy:[3]	$0.30T + 1.30T^3$
lead/tin film:	negligible in superconducting state
Total:	$0.5T + 1.4T^3$ erg/K

(2) Heater composed of

2.8 cm of 0.0025 cm diameter Pt/W wire:[55]	$0.05T + 3.4 \times 10^{-5}T^{-2}$ erg/K
2 cm of 0.01 cm diameter Ni wire:[56]	$0.1T^3$ (superconducting state)
Total:	$3.4 \times 10^{-5}T^{-2} + 0.05T + 0.1T^3$ erg/K

(3) 0.001 g GE 7031 varnish:[57] $0.07T + 0.2T^3$ erg/K

(4) Fishing line (nylon), 0.01 g (see comment below): $0.5T + 2T^3$ erg/K

Addenda total = $C_a = 3.4 \times 10^{-5}T^{-2} + 1.1T + 3.7T^3$ erg/K

We have for $T = 0.1$ K, $C_a/T^3 = 117$ erg/K^4, and for $T = 0.3$ K, $C_a/T^3 = 16$ erg/K^4. From Fig. 4, the excess over line A is 150 erg/K^4

at 0.1 K and 17 erg/K^4 at 0.3 K. Thus C_a accounts in a rough way for the measured heat capacity. It should be noted that the fishing line, which makes up $\approx$50% of the addenda mass, has never been independently measured. However, it is an amorphous material,[58] and so the specific heat of epoxy has simply been assumed.

The heat capacity curve for sample 0 h (unannealed, mass 5.34 g) in Fig. 4 is fitted well by the following expression:

$$C/T^3 = 1.54T^{-1.99} + 31.8 \text{ erg/K}^4$$
$$= C_a/T^3 + C_{xtal}/T^3$$

where C_a/T^3 is the addenda heat capacity divided by T^3 (to be fitted; not identical with the estimated C_a above), and C_{xtal}/T^3 is the contribution of the quartz crystal. C_{xtal} is assumed to be entirely Debye-phonon-like (i.e., $C_{xtal} \propto T^3$). The $1.54T^{-1.99}$ term has the temperature dependence of a glass, which is to be expected since the addenda is almost all amorphous. The constant portion of C_a/T^3 is estimated by assuming that the curve C_a/T^3 has the same general shape as the specific heat curve for vitreous silica for $T \lesssim 4$ K. (Equivalently, it is assumed that the average velocity of sound in the addenda is similar to that in vitreous silica). We find

$$C_a/T^3 = 1.54T^{-1.99} + 0.9 \text{ erg/K}^4$$

which leaves for the quartz crystal,

$$C_{xtal}/T^3 = 30.9 \text{ erg/K}^4$$

The above C_{xtal}/T^3 corresponds to a Debye phonon heat capacity, phonons of average velocity $\bar{v} = 4.4 \times 10^5$ cm/s, which agrees with the average value computed from elastic constants.[11]

It should be noted that the fit to the addenda for $T > 0.6$ K is not critical, since the glass-like excitations measured in the samples are dominant in the $T \lesssim 0.5$ K range.

Finally, we note that for the diffusivity technique, the addenda heat capacity was negligible. No fishline was used, and the thermometer was constructed half as massive as the weak-link thermometer. Hence, the addenda heat capacity was cut by a factor of 4, and would contribute only about 2% to the measured specific heat of sample 270 h or 2100 h in any temperature range.

APPENDIX B

THERMAL CONDUCTIVITY LIMITED BY INCLUSIONS

In the Boltzmann and Debye approximations, the following expression gives the thermal conductivity κ in the low-temperature limit ($T \ll T_{Debye}$, $T_{Debye} \sim 500$ K for quartz[11,59]) if the mean free path as a function of frequency, $\ell(\omega)$, is known:

$$= A\, T^3 \int_0^{\infty} \frac{x^4\, e^x\, dx}{(e^x - 1)^2}\, \ell(2\pi kTx/h)$$

where $A = \frac{1}{3}(\sum_{i=1}^{3} v_i^{-2})\ 1.57 \times 10^9$ W cm^{-2} K^{-4} if the velocity v of the ith polarization phonon is expressed in cm/s and ℓ is expressed in cm. The k and h are Boltzmann's constant and Planck's constant, respectively. For quartz,[11] $A = 8.7 \times 10^{-3}$ W cm^{-2} K^{-4}.

The sample 0 h conductivity fits in Fig. 5 were derived from the following mean free paths (see p. 25):

Before anneal:
$\ell_B = 0.81$ cm
$\ell_I = 2.2 \times 10^{-46}$ cm s^{-4} ω^{-4}, $\omega < 6.5 \times 10^{11}$ s^{-1}
$\ell_I = 0.027$ cm, $\omega > 6.5 \times 10^{11}$ s^{-1}

After anneal:
$\ell_B = 0.81$ cm
$\ell_I = 1.4 \times 10^{-43}$ cm s^{-4} ω^{-4}, $\omega < 1.3 \times 10^{11}$ s^{-1}
$\ell_I = 0.045$ cm, $\omega > 1.3 \times 10^{11}$ s^{-1}

APPENDIX C

SPECIFIC HEAT DATA

This appendix lists the heat capacity and specific heat data by sample. The unit of temperature T is Kelvin (K). If the weak-link method was used, the volume of the sample is given, and C'/T^3 denotes the heat capacity of the sample with addenda, divided by T^3, in units erg/K^4. The column C/T^3 is the specific heat (divided by T^3) of the sample only. Subtraction of the addenda heat capacity is described in Appendix A. The units of the specific heat divided by T^3 are erg cm^{-3} K^{-4}. For data taken by the diffusivity method, column C/T^3 is specific heat (divided by T^3). The heat capacity of the diffusivity addenda was negligible, as discussed in Appendix A. The scale factor (see p. 18) for the diffusivity specific heat is given; the listed data are not scaled.

0 h, 2.015 cm^3

T	C'/T^3	T	C'/T^3	T	C'/T^3
0.0985	174	0.1680	86.3	0.396	38.2
.1032	153	.1759	82.9	.534	36.7
.1077	149	.1834	76.5	.557	36.6
.1090	148	.1910	73.4	.660	34.1
.1125	140	.2026	68.1	.797	33.6
.1198	136	.2234	61.4	.811	35.3
.1261	122	.2402	55.9	.979	34.6
.1320	123	.2674	50.7	1.123	33.1
.1383	113	.2923	50.8	1.390	32.6
.1461	106	.304	45.7		
.1510	101	.331	45.2		
.1510	97.0	.342	42.2		
.1582	94.2	.368	41.6		

0 h annealed 840°C, 1.874 cm^3

T	C'/T^3	C/T^3
0.1102	687	300
.1251	506	219
.1513	328	140
.1879	206	87.6
.256	122	52.9
.404	59.7	26.9
.408	58.0	26.0
.748	35.3	17.1
1.052	31.7	15.7
1.990	32.0	16.4
6.26	34.4	17.7

3h, 2.000 cm^3

T	C'/T^3	C/T^3	T	C'/T^3	C/T^3
0.1362	379	149	0.397	68.5	29.0
.1370	358	138	.523	66.7	30.1
.1389	340	131	.733	82.9	39.6
.1529	299	117	.836	103	50.0
.1558	262	99.2	.946	103	50.1
.1687	244	95.0	1.057	103	50.5
.1688	234	90.2	1.249	92.0	45.1
.1929	182	70.4	1.674	73.3	35.9
.209	161	62.6	2.33	49.7	24.3
.255	117	46.4	4.18	36.7	17.8
.293	97.7	39.5	7.30	39.6	19.1

3 h annealed 370°C, 2.00 cm^3

T	C'/T^3	C/T^3	T	C'/T^3	C/T^3
0.1366	330	124	0.631	73.7	34.5
.1676	219	82.1	.895	102	49.7
.1949	157	58.1	1.056	110	53.9
.221	119	43.6	1.205	108	53.0
.296	68.2	25.0	1.678	78.2	38.4
.396	56.4	22.9	3.03	41.5	20.2
.399	55.8	22.7			

3 h annealed 840°C, 2.00 cm^3

T	C'/T^3	C/T^3	T	C'/T^3	C/T^3
0.1261	609	257	0.257	138	57.1
.1364	497	208	.315	97.8	40.8
.1366	505	212	.399	67.7	28.6
.1367	508	213	.525	49.9	21.7
.1507	393	163	.731	39.0	17.6
.1670	315	130	1.045	35.8	16.7
.1908	241	99.3	1.674	34.7	16.5
.1908	234	95.8	2.39	34.4	16.6
.220	180	74.0	6.24	38.5	18.7

27 h, 2.01 cm^3

T	C'/T^3	C/T^3
0.218	247	107
.240	250	111
.244	229	101
.271	209	93.7
.299	196	89.1
.306	174	78.6
.328	165	75.2
.378	158	73.1
.409	151	70.4
.427	165	78.0
.485	177	84.9
.531	211	102
.537	209	102
.538	210	102
.553	230	112
.562	259	127
.584	257	126
0.593	266	130
.597	269	132
.650	325	160
.656	337	166
.682	360	178
.689	374	181
.729	385	190
.742	388	192
.808	456	226
.838	476	236
.858	483	239
1.017	521	258
1.187	519	258
1.507	381	189
1.732	298	148
2.62	110	54.6
3.01	78.9	39.1

27 h annealed 840°C, 1.811 cm^3

T	C'/T^3	C/T^3
0.1905	118	41.6
.204	107	38.4
.211	99.1	35.4
.228	88.6	32.4
.252	77.6	29.1
.279	70.2	27.5
.316	60.1	24.3
.397	47.8	20.5
.518	39.4	18.1
.883	34.5	17.5
1.276	32.5	16.9

270 h, 2.108 cm^3

T	C'/T^3	C/T^3	T	C'/T^3	C/T^3
0.359	321	147	0.751	920	435
.393	319	146	.960	1110	527
.413	339	157	.960	1090	515
.443	346	160	1.066	1160	549
.460	377	175	1.198	1120	530
.536	471	221	1.475	941	446
.639	671	316	1.854	531	252

270 h annealed 370°C (1 h), scale factor 0.55

T	C/T^3	T	C/T^3
0.1890	1150	0.417	419
.207	1000	.443	453
.227	874	.540	586
.250	786	.614	718
.275	675	.720	886
.303	600	1.050	1150
.332	500	1.171	1100
.370	445		

270 h annealed 840°C, 2.102 cm^3

T	C'/T^3	C/T^3	T	C'/T^3	C/T^3
0.288	416	189	0.555	241	112
.317	367	167	.610	242	113
.349	321	147	.740	268	126
.374	297	136	.899	293	139
.402	265	122	1.049	300	142
.436	248	114	1.068	288	136
.445	229	105	1.307	234	111
.487	234	108	1.499	200	94.6
.501	240	111			

270 h annealed 840°C, scale factor 0.80

T	C/T^3	T	C/T^3
0.1930	512	0.360	181
.229	348	.438	142
.229	343	.573	127
.260	312	.784	149
.273	288	1.042	159
.316	216	1.314	127
.316	217		

2100 h, scale factor 0.85

T	C/T^3	T	C/T^3
0.1804	344	1.042	82.1
.1976	297	1.191	79.5
.216	256	1.422	64.0
.226	230	1.630	52.9
.237	215	1.910	45.5
.286	164	2.59	31.1
.368	107	3.05	29.5
.436	83.5	3.59	28.4
.547	68.9	4.73	30.7
.675	81.6	4.86	31.5
.823	81.6	6.02	41.1

2100 h annealed 370°C, 2.24 cm^3

T	C'/T^3	C/T^3
0.732	93.5	40.1
.828	84.8	36.5
1.044	71.9	31.1
1.044	72.5	31.3
1.662	58.3	25.4
2.74	54.9	24.0
4.92	67.3	29.5

2100 h annealed 370°C, scale factor 0.85

T	C/T^3
0.1890	319
.228	254
.249	200
.298	145
.386	101
.830	41.4
1.050	36.7
1.700	29.9
7.34	44.8

APPENDIX D

THERMAL CONDUCTIVITY DATA

This appendix lists the thermal conductivity data by sample. The unit of temperature T is Kelvin (K). The units of thermal conductivity κ are W cm^{-1} K^{-1}. "E-n" following a number denotes x 10^{-n}, where n is some integer. Unless otherwise noted, the conductivity was measured in the "central region" (as defined in Chapter II, A.). The rectangular cross section of each sample is given in units cm x cm.

0 h, 0.403 x 1.006

T	K	T	K
0.0470	1.89E-5	0.274	2.61E-3
.0519	2.56E-5	.393	5.81E-3
.0578	3.48E-5	.471	8.32E-3
.0630	4.49E-5	.519	1.00E-2
.0692	5.89E-5	.566	1.16E-2
.0763	7.80E-5	.726	1.74E-2
.0837	1.02E-4	.971	2.71E-2
.0919	1.34E-4	1.332	4.45E-2
.1114	2.28E-4	1.636	6.46E-2
.1325	3.80E-4	1.938	8.79E-2
.1595	6.25E-4	2.49	1.44E-1
.1907	1.02E-3	3.25	2.48E-1
.228	1.64E-3		

0 h annealed 840°C, 0.403 x 1.006

T	K	T	K
0.0471	1.67E-5	0.1536	1.78E-4
.0526	2.17E-5	.201	3.03E-4
.0580	2.69E-5	.232	4.11E-4
.0635	3.28E-5	.324	8.49E-4
.0700	3.99E-5	.587	3.35E-3
.0833	5.60E-5	.949	1.03E-2
.0980	7.62E-5	1.960	5.27E-2
.1148	1.02E-4	3.09	1.47E-1
.1330	1.34E-4		

0 h annealed 840°C, outside region, 0.403 x 0.451

T	K	T	K
0.0454	1.39E-5	0.206	1.29E-3
.0529	2.22E-5	.299	3.81E-3
.0616	3.53E-5	.411	9.47E-3
.0703	5.31E-5	.512	1.81E-2
.0897	1.12E-4	.675	3.97E-2
.1292	3.28E-4	1.107	1.72E-1
.1547	5.56E-4		

3 h, 0.403 x 0.998

T	κ	T	κ
0.0533	1.77E-5	0.244	1.00E-3
.0678	3.37E-5	.325	1.86E-3
.1021	1.05E-4	.494	4.12E-3
.1186	1.51E-4	.617	5.96E-3
.1357	2.22E-4	1.004	1.29E-2
.1548	3.23E-4	1.596	2.68E-2
.1896	5.46E-4	2.05	4.00E-2

3 h annealed 840°C, 0.403 x 0.998

T	κ	T	κ
0.0438	1.06E-5	0.1532	1.42E-4
.0482	1.26E-5	.1997	2.52E-4
.0532	1.60E-5	.228	3.35E-4
.0614	2.20E-5	.325	7.78E-4
.0720	3.32E-5	.584	3.31E-3
.0826	4.20E-5	.940	1.07E-2
.0994	6.03E-5	1.426	2.83E-2
.1142	7.90E-5	1.929	5.74E-2
.1329	1.07E-4	3.04	1.59E-1

27 h, 0.403 x 1.006

T	K	T	K
0.0536	1.09E-5	0.253	4.11E-4
.0689	2.08E-5	.329	7.09E-4
.1032	5.25E-5	.613	2.33E-3
.1183	7.25E-5	.823	3.92E-3
.1185	7.32E-5	1.185	7.63E-3
.1381	1.05E-4	1.545	1.15E-2
.1404	1.09E-4	1.740	1.31E-2
.1615	1.50E-4	2.00	1.65E-2
.1951	2.31E-4		

27 h annealed 840°C, 0.403 x 1.006

T	K	T	K
0.0590	1.36E-5	0.1963	2.14E-4
.0742	2.35E-5	.224	2.96E-4
.0853	3.21E-5	.322	7.30E-4
.1001	4.65E-5	.588	3.32E-3
.1136	6.11E-5	.945	1.06E-2
.1330	8.68E-5	1.944	5.13E-2
.1499	1.14E-4	3.07	1.25E-1

27 h annealed 840°C, outside region, 0.403 x 0.446

T	K	T	K
0.0481	1.16E-5	0.1046	1.16E-4
.0570	2.02E-5	.1537	3.55E-4
.0626	2.61E-5	.1674	4.54E-4
.0729	4.06E-5	.230	1.12E-3
.0901	7.76E-5	.313	2.72E-3

270 h, 0.409 x 1.026

T	K	T	K
0.1091	5.01E-6	0.557	1.07E-4
.1246	6.29E-6	.962	2.77E-4
.1529	9.47E-6	2.11	8.58E-4
.1704	1.17E-5	3.16	1.29E-3
.201	1.62E-5	5.86	2.09E-3
.230	2.10E-5	7.78	2.16E-3
.342	4.44E-5		

270 h annealed 840°C, 0.410 x 1.026

T	K	T	K
0.1045	5.06E-6	0.806	1.62E-4
.1203	6.50E-6	1.213	2.69E-4
.1379	8.39E-6	1.365	3.10E-4
.1592	1.10E-5	2.19	4.91E-4
.1841	1.44E-5	2.61	5.59E-4
.211	1.85E-5	3.09	6.26E-4
.261	2.73E-5	4.74	7.89E-4
.351	4.55E-5	6.91	9.11E-4
.522	8.58E-5	7.30	9.26E-4

2100 h, 0.420 x 1.058

T	K
0.1622	1.56E-5
.1872	2.01E-5
.215	2.62E-5
.247	3.37E-5
.286	4.48E-5
.333	5.97E-5
.518	1.36E-4
.622	1.90E-4
.849	3.36E-4
.854	3.37E-4
1.066	5.01E-4
2.11	1.47E-3
3.17	2.40E-3
4.36	3.26E-3
5.99	4.11E-3
7.62	4.43E-3

2100 h annealed 370°C, 0.420 x 1.058

T	K
0.175	1.76E-5
.237	3.1E-5
.830	3.0E-4
7.34	4.0E-3

REFERENCES

1. R. B. Stephens, Phys. Rev. B13, 852 (1976).

2. W. A. Phillips, J. Non-Crystal. Solids 31, 267 (1978).

3. D. S. Matsumoto, C. L. Reynolds, Jr., and A. C. Anderson, Phys. Rev. B19, 4277 (1979).

4. J. E. Graebner, B. Golding, R. J. Schutz, F. S. L. Hsu, and H. S. Chen, Phys. Rev. Lett. 39, 1480 (1977).

5. P. W. Anderson, B. I. Halperin, and C. M. Varma, Philos. Mag. 25, 1 (1972).

6. W. A. Phillips, J. Low Temp. Phys. 7, 351 (1972).

7. R. C. Zeller and R. O. Pohl, Phys. Rev. B4, 2029 (1971).

8. R. B. Stephens, Ph.D. Thesis (Cornell University, 1974), unpublished.

9. P. Flubacher, A. J. Leadbetter, J. A. Morrison, and B. P. Stoicheff, J. Phys. Chem. Solids 12, 53 (1959).

10. N. Bilir and W. A. Phillips, Philos. Mag. 32, 113 (1975).

11. R. C. Zeller, M.S. Thesis (Cornell University, 1974), unpublished.

12. V. Narayanamurti and R. O. Pohl, Rev. Mod. Phys. 42, 201 (1970).

13. M. W. Klein, B. Fischer, A. C. Anderson, and P. J. Anthony, Phys. Rev. B18, 5887 (1978).

14. T. L. Smith, P. J. Anthony and A. C. Anderson, Phys. Rev. B17, 4997 (1978).

15. R. Berman, Proc. Roy. Soc. A208, 90 (1951).

16. M. C. Wittels, Philos. Mag. 2, 1445 (1957).

17. M. C. Wittels and F. A. Sherril, Phys. Rev. 93, 1117 (1954).

18. C. Laermans, Phys. Rev. Lett. 42, 250 (1979).

19. S. Hunklinger and W. Arnold, in Physical Acoustics, edited by W. P. Mason and R. N. Thurston (Academic, New York, 1976), Vol. 12, p. 155.

20. B. Golding and J. E. Graebner, in Phonon Scattering in Condensed Matter, H. J. Maris, ed. (Plenum, New York, 1980), p. 11.

21. C. Laermans and B. Daudin, in Phonon Scattering in Condensed Matter, H. J. Maris, ed. (Plenum, New York, 1980), p. 21.

22. D. S. Billington and J. J. Crawford, Radiation Damage in Solids (Princeton University, Princeton, 1961), pp. 13-14 (E_p = 1.5 MeV average for a fast neutron); p. 233.

23. W. Primak, The Compacted States of Vitreous Silica (Gordon and Breach, New York, 1975), p. 89.

24. Grown by Sawyer Research Products, Inc., Eastlake, Ohio; supplied by Valpey-Fisher Corporation, Hopkinton, Mass. The manufacturer provides the following list of typical impurity levels in ppm (wt.): Al, 15-55; Fe, 2-12; Na, 3-8; Li, 3-7; Mg, 1-2; Cu, 1-2.

25. Hole VT-8, 12" position from bottom of thimble was used.

26. G. Schulke, private communication. The pattern will be shown to originate from possible growth imperfections.

27. T. L. Smith, Ph.D. Thesis (University of Illinois, 1979), unpublished.

28. G. J. Sellers and A. C. Anderson, Rev. Sci. Instrum. 45, 1256 (1974).

29. This does not account for possible error in addenda subtraction.

30. The half-life of the radioactivity, as measured with a geiger counter, was found to be at least several years. The measurements of specific heat were performed within ~couple months after the thermal conductivity was measured; hence no time-dependence in the gradient is expected. A weaker assumption is that the same gradient is set up in the diffusivity configuration as in the thermal conductivity configuration. In the conductivity experiment, the sample-grease-refrigerator contact area was 2-3 times the sample-epoxy-refrigerator contact area in the diffusivity experiment. Hence the thermal gradient may have been larger than assumed in the diffusivity configuration. This would cause the average temperature to be higher than that calculated.

31. E. V. Kolontsova, A. E. Korneev, and V. P. Lutsenko, Sov. Phys. Dokl. 24(7), 556 (1979).

32. E. V. Kolontsova and I. V. Telegina, Sov. Phys. Solid State 7, 2207 (1966).

33. W. Primak, Phys. Rev. 110, 1240 (1958).

34. We use the "dominant phonon approximation:" the peak of the Bose-Einstein phonon distribution occurs at a phonon frequency $\nu \approx 10^{11}$ T Hz, T in Kelvin. Then 10^{11} T = velocity ($\sim 4 \times 10^5$ cm/s)/wavelength.

35. M. P. Zaitlin and A. C. Anderson, Phys. Rev. B12, 4475 (1975).

36. M. P. Zaitlin, L. M. Sclerr, and A. C. Anderson, Phys. Rev. B12, 4487 (1975).

37. D. Walton, Phys. Rev. 157, 720 (1967).

38. "Schottky two-level specific heat" refers to the specific heat of a density, N, of non-interacting two-level systems, all with energy splitting E: $C_S = Nk(E/2kT)^2 \mathrm{sech}^2(E/2kT)$, where k is Boltzmann's constant.

39. By way of example, the behavior of a sharp energy distribution of tunneling systems in alkali halides is given in Ref. 12. A strong dip in the thermal conductivity occurs near the temperature of the peak in the specific heat. We note that the coupling strength of glass-like excitations to the lattice is similar to that of the above tunneling systems [B. Fischer and M. W. Klein, Phys. Rev. Lett. 43, 289 (1979)]. Even so, a sufficiently sharp density of states would not affect the conductivity. The excellent fit of our Schottky curve implies (Ref. 12) a width in the density of states of $\lesssim 0.1$ K. Hence, it is unlikely that the Schottky excitations are causing the broadly lowered thermal conductivity of the 3 h and 27 h samples compared to the 0 h sample (all before anneal).

40. H. von Lohneysen and M. Platte, Z. Phys. B36, 113 (1979).

41. J. C. Lasjaunias, G. Penn, A. Ravex, and M. Vandorpe, J. Phys. (Paris) 41, L131 (1980).

42. J. Chaussy, J. Le G. Gilchrist, J. C. Lasjaunias, M. Saint-Paul, and R. Nava, J. Phys. Chem. Solids 40, 1073 (1979).

43. J. A. Weil, Radiation Effects 26, 261 (1975).

44. Despite the different expressions for the thermal conductivities of sample 270 h before and after anneal, the conductivities were the same within $\approx 5\%$ from 0.1-0.5 K.

45. From Ref. 14, $C_g = (46.0 \pm 2.3)\ T^{1.35 \pm 0.05} - 17.8\ T^3$ erg cm^{-3} K^{-1} for $T < 0.6$ K; $\kappa_g = (1.61 \pm 0.05) \times 10^{-4}\ T^{1.81 \pm 0.05}$ Wcm^{-1}K^{-1}, $T<1$ K.

46. We have assumed "η" is the same for all samples. See Ref. 14.

47. The conclusion holds also for 3 h before anneal and for 3 h after the 370°C anneal: the specific heat in all cases is large.

48. The conductivity of the annealed outer region of sample 0 h was used in Eq. 2. The 0 h outer sample possessed the same cross section as the 27 h outer sample. There is no ambiguity from "inclusion" scattering: no inclusion scattering was observed in the 0 h outer region (Fig. 5).

49. This may suggest that the production of glass-like excitations by the neutron irradiation is a function of the original perfection of the crystal.

50. See Billington, Ref. 22, p. 252 (magnetic centers), p. 259 (extinction coefficient).

51. In the tunneling states model, $\kappa \propto n^{-1}$, where n is the (approximately) energy-independent density of glass-like excitations.

52. If $\kappa_g \propto T^{2-n}/\gamma_g^2$ and $\kappa_x \propto T^{2-m}/\gamma_x^2$, where g and x refer respectively to vitreous silica and an irradiated quartz sample, the tunneling states model assumes $n_g(E) \propto E^n$ and $n_x(E) \propto E^m$, where n is the number of excitations per unit energy per unit volume. Therefore, assuming $\gamma_g = \gamma_x$, the number of excitations per unit volume up to 1 K in sample x is $\int_0^{1\ K} n_x(E)dE = \int_0^{1\ K} n_g(E)\frac{\kappa_g(E)}{\kappa_x(E)}dE$, E in Kelvin units. From Ref. 14, $n_g(E) = 1.04 \times 10^{33} E^{0.35}$ erg^{-1} cm^{-3} if E is expressed in Kelvin.

53. In particular, the cause of the "plateau" in κ is not known, and the specific heat above 1 K becomes dominated by phonons with non-simple dispersion relations.

54. B. J. C. Van Der Hoeven, Jr., and P. H. Keesom, Phys. Rev. 130, 1318 (1963).

55. J. C. Ho and N. E. Phillips, Rev. Sci. Instrum. 36, 1382 (1965).

56. G. J. Sellers, Ph.D. Thesis (University of Illinois, 1975), unpublished.

57. R. B. Stephens, Cryogenics 15, 420 (1975).

58. A. C. Anderson, private communication.

59. C. Kittel, Introduction to Solid State Physics, 4th ed. (John Wiley & Sons, New York, 1971), p. 215.

VITA

John William Gardner was born in [redacted] He received a Bachelor of Arts degree from Princeton University in Princeton, New Jersey, in 1976 and a Master of Science degree from the University of Illinois at Urbana-Champaign in 1978.